Performance Evaluation of Ground Heating and Cooling Systems

Long-term performance measurements of two case buildings

Hao Liu and Hongyi Zhang

Master thesis in Energy-efficient and Environmental Buildings

Lund University

Lund University, with eight faculties and a number of researches centres and specialized institutes, is the largest establishment for research and higher education in Scandinavia. The main part of the University is situated in the small city of Lund which has about 112 000 inhabitants. A number of departments for research and education are, however, located in Malmö. Lund University was founded in 1666 and has today a total staff of 6 000 employees and 47 000 students attending 280 degree programmes and 2 300 subject courses offered by 63 departments.

Master Programme in Energy-efficient and Environmental Building Design

This international programme provides knowledge, skills and competencies within the area of energy-efficient and environmental building design in cold climates. The goal is to train highly skilled professionals, who will significantly contribute to and influence the design, building or renovation of energy-efficient buildings, taking into consideration the architecture and environment, the inhabitants' behaviour and needs, their health and comfort as well as the overall economy.

The degree project is the final part of the master programme leading to a Master of Science (120 credits) in Energy-efficient and Environmental Buildings.

Examiner: Dennis Johansson (Building Services)

Supervisor: Saqib Javed (Building Services)

Keywords: ground source heat pump (GSHP), system performance, long-term monitoring, geothermal, borehole heat exchangers, office building, uncertainty analysis, Deep Green Cooling, free cooling, heating, cooling

Thesis: EEBD - 20/07

Abstract

Geothermal energy is one of the oldest and most sustainable energy sources and has been used for thousands of years. The temperature of the ground at shallow depth is fairly constant, above the air temperature in winter and lower than the ambient temperature in summer. Shallow geothermal energy systems can thus be used to provide heating and cooling with or without heat pumps.

This study aims to analyse the long-term performance measurements of two shallow geothermal heating and cooling systems. The first system is installed in a small clubhouse in Gothenburg, whereas the second system is installed in a large office building in Stockholm. For both installations, high-frequency data has been collected for several years, which enables evaluating and analyzing the performance of these systems.

The first system provides space heating and domestic hot water (DHW). It is a water-to-water heat pump connected to a single 230-m deep borehole heat exchanger. This study uses long-term high-frequency measurement data from this clubhouse and investigates the energy performance of the GSHP system for the three years between 2014–2016.

The second system is installed at the Entré Lindhagen in Stockholm. The system is primarily a direct ground cooling system but also preheats the ventilation air to balance the ground loads. The system was taken into operation in January 2014 and serves a heated floor area of 65,265 m². The ground system consists of 144 boreholes with double U-tubes, each with an active-depth of 220 m. This study provides the performance evaluation of the ground system for five years between 2014–2018 using high-frequency measurement data.

Within the scope of this work, seasonal performance factors for both systems are evaluated corresponding to the SEasonal PErformance factor and MOnitoring (SEPEMO) and/or Annex 52 system boundary schemes. Results are analysed to show how the various system components affect performance. The outcome of this research provides a set of benchmarks for comparison of such systems around the world.

Preface

This work was the Degree Project and the final part of the Energy-Efficient and Environmental Building Design Master program at Lund University. Besides, this work is part of the IEA HPT Annex 52, long term performance measurement of GSHP systems serving commercial, institutional, and multi-family buildings. It was carried out at the Division of Building Services.

Acknowledgements

We would like to take the opportunity to express our sincere gratitude towards our supervisor Saqib Javed from the Division of Building Services. Thank you for providing us with this opportunity to do this research. Without your constant support, guidance, and encouragement it would not have been possible to complete this thesis to the best of our ability.

We also extend our special thanks to Jonas Gräslund from Skanska Commercial Development Nordic for providing Entré Lindhagen Building data and answering our questions. Besides, we extend our thanks to Håkan Larsson from the Chalmers University of Technology for helping with Sisjön measurements.

Finally, we would like to acknowledge Maria Wall, the director of the Energy-efficient and Environmental Building Design (EEBD) Master's Programme, and all the course teachers for sharing their valuable knowledge.

2020, Helsingborg

Hao Liu and Hongyi Zhang

Abbreviations and Symbols

Nomenclature	Explanation
$e_{\Delta T}$	Fractional uncertainty of the temperature difference
$e_{\dot{V}}$	Fractional uncertainty of the flow rate
$e_{\dot{V},w}$	Fractional uncertainty of the water flow rate
$e_{\dot{V},b}$	Fractional uncertainty of the brine flow rate
$e_{W,n}$	Fractional uncertainty of the electrical energy use for the period *n*
e_Q	Fractional uncertainty of the thermal energy
e_q	Fractional uncertainty of the heat transfer rate
$e_{Q,n}$	Fractional uncertainty of the thermal energy for the period *n*
$e_{SPF,n}$	Fractional uncertainty of the SPF value for the period *n*
$E_{\Delta T}$	Absolute uncertainty of the temperature difference (K)
E_{ah}	Absolute uncertainty of the electrical use of auxiliary heater (kWh)
E_c	Absolute uncertainty of the electrical use of compressor (kWh)
E_{Fan}	Absolute uncertainty of the electrical use of fan (kWh)
$E_{p,d}$	Absolute uncertainty of the electrical use of distribution pump (kWh)
$E_{p,l}$	Absolute uncertainty of the electrical use of load pump (kWh)
$E_{p,s}$	Absolute uncertainty of the source pump electrical energy use (kWh)
E_W	Absolute uncertainty of the electrical use (kWh)
$E_{W,n}$	Absolute uncertainty of the electrical energy use for the period *n* (kWh)
E_Q	Absolute uncertainty of the hourly thermal energy (kWh)
E_q	Absolute uncertainty of the hourly heat transfer rate (kWh)
$E_{Q,n}$	Absolute uncertainty of the thermal energy for the period *n* (kWh)
$Energy_{coil,A}$	Fan energy use due to coil A (kWh)
$Energy_{total}$	Total fan energy use (kWh)
q	Heat transfer rate (W)
Q	Heat energy transfer (kWh)
Q_{ah}	Thermal energy output of auxiliary heating (kWh)
Q_{ghe}	Thermal energy output of ground heat exchanger (kWh)
Q_{del}	Thermal energy output of delivered energy (kWh)
Q_r	Thermal energy output of the refrigeration cycle (kWh)
W	Electrical energy use (kWh)
W_{ah}	Electrical energy use of auxiliary heating (kWh)
W_{Fan}	Electrical energy use of fan (kWh)
W_c	Electrical energy use of the compressor (kWh)
$W_{p,s}$	Electrical energy use of the source-side pump (kWh)
$W_{p,l}$	Electrical energy use of the load-side pump (kWh)
$\Delta P_{coil,A}$	Pressure drop of the coil A (Pa)
ΔP_{total}	Total pressure drop of all coils (Pa)

Abbreviation	Explanation
ASHP	Air source heat pump
DHW	Domestic hot water
DGC	Deep green cooling
GSHP	Ground source heat pump
HVAC	Heating ventilation and air conditioning
ODA	Outdoor air temperature
SEPEMO	SEasonal PErformance factor and MOnitoring for heat pump systems
SPF	Seasonal performance factor

Symbol		Explanation
		Ground heat exchanger
		Circulation pump
		Chilled beam
		Domestic hot water
		District heating
		Electric heater
		Electrical energy meter
		Fan
		City water
		Flow meter
		Heat exchanger
		Heat recovery
		Radiator
		Refrigeration Cycle
		Temperature sensor
		Water tank

Table of content

Abstract I
Preface III
Acknowledgements V
Abbreviations and Symbols VII
Table of content IX

1 Introduction 1
1.1 Background 1
1.2 Aim and objectives 2
1.3 Limitations 2
1.4 Disposition of the thesis 3

2 Literature Review 5
2.1 Ground heating and cooling system performance 5
2.2 Ground heating and cooling system issues and solutions 7
2.3 Comparison of ground-source and air-source systems 8

3 Method 9

4 Case study 1 11
4.1 System description 11
4.2 Measurements 12
4.3 System boundaries 14
4.4 Uncertainty analysis 17
4.4.1 Thermal energy 17
4.4.2 Electrical energy use 18
4.4.3 Seasonal performance 19
4.5 Results 19
4.5.1 Ground heat exchange and load characteristics 19
4.5.2 Energy performance 21
4.5.3 Seasonal performance factors 23
4.5.4 Further analysis 27

5 Case study 2 29
5.1 System description 29
5.2 Measurements 31
5.3 System boundaries 32
5.4 Uncertainty analysis 34
5.4.1 Thermal energy 34
5.4.2 Electrical energy Use 35
5.4.3 Seasonal performance 35
5.5 Results 35
5.5.1 Ground heat exchange and load characteristics 36
5.5.2 Energy performance 40
5.5.3 Seasonal performance factors 43

6 Discussion and Conclusions 47

References 51

1 Introduction

This chapter provides the necessary background for this study. It also presents the aim and objectives, and the limitations of the work.

1.1 Background

Buildings in developed countries account for around 40 % of the energy consumption and attribute to approximately 40 % of the carbon dioxide emissions (Pérez-Lombard et al., 2008; Gleeson and Lowe, 2013). With an ever-increasing emphasis on environmental protection and the efficient use of energy, an extensive amount of research is now focused on reducing both the environmental impacts and the energy consumption of the buildings (de Klijn-Chevalerias and Javed, 2017; Hassan and Javed, 2019). All new buildings in the EU have to meet the requirements of nearly Zero Energy Buildings (nZEB) by 2021 (European Parliament, 2010). To comply with these requirements, both energy efficiency and on-site energy production technologies must be combined (Wemhoener et al., 2017). Among the novel and renewable energy sources and technologies, geothermal heating and cooling are regarded as a promising technology offering both environmental benefits and high energy efficiency (Rees, 2016).

The use of shallow geothermal energy systems has increased several folds over the past decades (Vieira et al., 2017). The installed geothermal power for direct utilization in the world increased from 48,485 MW_t in 2010 to 70,885 MW_t in 2015. Meanwhile, the thermal energy supplied by these systems also increased significantly from 423,918 TJ/year in 2010 to 592,638 TJ/year in 2015 (Lund and Boyd, 2015). In Europe, the shallow geothermal energy systems account for the largest share of installed capacity among the three geothermal sub-sectors of shallow applications, direct use, and electrical energy production. The shallow geothermal energy use in Europe is currently approximately 26,923 MW_{th} (Sanner, 2019). Sweden has the highest number of installed shallow ground source heat pump (GSHP) systems and also has the largest installed capacities in Europe, followed by Germany, Finland, France, and Switzerland. There are currently over 580,000 GSHP systems installed in Sweden. These systems together account for 22,950 GWh_{th}/year of annual energy production and constitute 6,520 MW_{th} installed capacities.

Compared to a few other renewable energy sources, which sometimes lack constant and secure energy supply, geothermal energy solutions offer excellent advantages of providing persistent heating and cooling throughout the year. The shallow geothermal systems use the ground as a source or sink of heat, thus taking advantage of the seasonally moderate temperatures in the shallow underground to boost efficiency and to reduce the operational costs of heating and cooling systems (Javed, 2012; Carlini and Castellucci, 2011). Furthermore, these systems can be installed almost everywhere and have a low operational cost. Hence, geothermal systems have been widely promoted and applied all over the world (Duque and Pascoal, 2014; Tsagarakis et al. 2020).

Despite the growing popularity and widespread use of geothermal heating and cooling systems, only a handful of studies have systematically examined the real-world performance of these systems. In some of the reported literature studies, the GSHP systems have been shown to be running unsatisfactorily or sub-optimally (Bockelmann and Fisch, 2019). In some

other studies, the energy performance of the studied systems has been shown to be lower than the expected values at the design stage (Li et al., 2014; Kurkinen et al., 2014; Geng et al., 2019). The reasons behind this under-performance include incorrect dimensioning of the system due to over-optimistic assumptions or user-dependent operational issues. As noted by Bockelmann and Fisch (2019), the ground source heating and cooling systems react very sensitively to incorrect dimensioning or user-dependent operational issues due to the small temperature difference between the ground and the heating or the cooling system. Moreover, to provide better energy efficiency and to ensure a comfortable indoor environment, several factors including, among others, optimization of the design, system control, and the operation strategy, have to be considered (Spitler and Gehlin, 2019).

The long-term field measurements of geothermal heating and cooling systems provide a unique opportunity to study system issues and to analyse their real-world system performance. It is, however, important to evaluate the performance consistently and systematically to make a fair comparison between different systems. Hence, standardised evaluation methods with defined system boundaries are vitally important for evaluating and comparing the performance of different geothermal heating and cooling systems.

1.2 Aim and objectives

The objective of this thesis is to evaluate the long-term performance of two geothermal heating and cooling systems in Sweden. The first building considered in this work is a clubhouse in Gothenburg with a ground source heat pump (GSHP) system providing domestic hot water (DHW) and space heating. High-resolution measurement data for the time period 2014–2016 collected by Chalmers University of Technology, with a sample interval of 2 minutes, has been used for this work. The second building used in this work is a low-energy office building in Stockholm with a direct ground cooling system. The system operates without any mechanical or thermal refrigeration system. Measurement data for the time period 2014–2018 provided by the building owners, with a sample interval of 5 minutes, has been used for this work.

The motivation of this work is to analyze the measured data and to determine the measured performance of the two systems according to the established methods of performance evaluation reported in the literature. The aim is to show how various system components affect system performance and to identifiy the operational strategies for achieving good efficiencies and superior system performances.

1.3 Limitations

The study evaluates the performance of the ground source heating and cooling system of two reference buildings. The system performance, as well as the energy use of the case studies, has been determined based on the long-term monitoring data provided by the project partners. All conclusions drawn in this report are based on the findings of these case studies and may not apply to other cases. The ambient-air temperature for the first case study was not measured on-site but obtained from a nearby weather station. In addition, the polynomial regression algorithm was used to fill some gaps in the measured data.

1.4 Disposition of the thesis

This master thesis first provides an extensive review of literature in Chapter 2 covering several system performance evaluation case studies of geothermal heating and cooling systems. In Chapter 3, a general methodology used in this thesis for evaluating and analyzing the seasonal performance has been presented. Chapter 4 and Chapter 5 present and describe the two case studies including the system boundaries, the uncertainties analysis, and the seasonal performance factors. Chapter 6 presents a comparative discussion of the seasonal performance factors and system operation results, together with conclusions and useful lessons for analysis and evaluation of geothermal heating and cooling systems.

2 Literature Review

Several studies related to geothermal heating and cooling system measurements have been published in the literature. The literature studies include previous case studies and monitoring experience from geothermal heating and cooling systems. The literature also presents measured system performances, applied evaluation procedures, as well as systematic issues and preventive measures for a few application examples.

2.1 Ground heating and cooling system performance

Miara et al. (2011) studied 110 heat pump systems using three years of measured data. The authors used a system boundary scheme with four different levels to evaluate system performance. The annual average seasonal performance factors (SPFs) for boundary 2 varied from 3.1 to 5.1 for the studied GSHP systems. This SPF boundary includes the borehole circulation pumps, heat pump unit, and the back-up heater. The work presented recommendations on improving the design, installation, and operation of the GSHP systems.

Stafford (2011) investigated the application of ground source heat pump systems in ten similarly constructed dwellings using one full year of monitoring data. The paper analyzed the impact of various energy consumption components using seven different system boundaries. One system boundary corresponded to the performance of the heat pump, borehole circulation pumps, and the auxiliary heaters. Under this system boundary, the annual SPF (for space heating and DHW) averaged over the ten systems was 2.38. The paper also concluded that the location of temperature measurement is vitally important, as it can result in inaccurate energy consumption estimates.

Michopoulos et al. (2013) presented the evaluation of a GSHP system in a Municipality Hall in Northern Greece based on eight-years of operation data. The GSHP system consists of 21 borehole heat exchangers, each 80-m deep, and 11 heat pump units. The authors reported the weekly performance factor as well as the seasonal energy efficient ratios of the heat pump systems. The performance factors were between 5.0–6.2 in heating mode and between 4.1–5.9 in cooling mode. The seasonal energy efficiency ratios were between 4.5–5.5 in heating mode and between 3.6–4.5 in cooling mode. However, the SPF boundaries were not well defined. Moreover, a maximum specific heat extraction rate of 50 W/m was measured in heating mode.

Mermoud et al. (2014) analyzed the performance of a GSHP system in a renovated office building in Geneva, Switzerland using SEPEMO boundary scheme. The system comprises of 11 boreholes, each 244-m deep. The paper reported the SPF4 value, representing the performance of the whole system, to be 3.0. The authors commented that the modest SPF values were due to the high temperature of the supply water.

Liu and Malhotra (2014) analyzed a GSHP system serving the heating system of a 2044 m^2 warehouse and an 864 m^2 truck bay in the Kalispell, US. The predicted and measured energy performance were compared and it was shown that the measured coefficient of performance (COP) value of the whole system in the peak load period was 2.66, which was similar to the

predicted value of 2.7. The paper also presented a combined cost and energy performance analysis of the system.

Luo et al. (2015) investigated the heating and cooling performance of a GSHP system in an office building in southern Germany. The system has 8 boreholes, each 80-m deep. The paper pointed out the cooling performance of this GSHP system was decreasing over time. It was due to unbalanced ground loads as the heat extraction from the ground was lower than the heat injection into the ground. Besides, the paper also showed that thermal energy loss in the distribution system could cause a significant reduction in the energy performance of the system.

Mendrinos and Karytsas (2016) reported on the Ground-Med project with GSHP systems installed in eight demonstration buildings to provide heating in winter, and free or compressor cooling in summer. The systems incorporated a number of novel features including an air-handling unit prototype utilizing condensing heat, prototypes of low-temperature fan-coil units, thermal storage units, as well as advanced control algorithms. The low-temperature heating and high-temperature cooling system solutions were implemented, supplying water at 28 ℃ to 43 ℃ for heating and at 7 ℃ to 18 ℃ for cooling. The system performance was evaluated, and the monthly values of SPF2, corresponding to the energy performance of compressors and external pumps, were reported. The SPF2 values in heating were between 3.63 and 5.91, in active cooling were between 4.87 and 6.76, and in free cooling modes were between 9.80 and 16.59.

Hughes (2018) studied 28 heat pump systems around the UK using the SEPEMO boundary scheme. The $SPF4_{heating}$ values, which represent the whole heating system performance, varied from 1.48 to 4.19 between different systems. The study demonstrated that design, installation, commissioning and operational aspects are all significant for an energy-efficient implementation. The study also pointed out that appropriate temperature levels are crucial for optimizing the performance.

At present, several long-term performance measurements of GSHP systems serving commercial, institutional and multi-family buildings are being analysed within the framework of the IEA HPT Annex 52 (Gehlin and Spitler, 2020). The evaluation of these systems is aimed at providing useful lessons and to suggest improvements for future projects. Among these are the systems studied by Naicker and Rees (2018), Bockelmann and Fisch (2019), and Spitler and Gehlin (2019). Naicker and Rees (2018) have performed a performance analysis of a large geothermal heating and cooling system comprising of fifty-six vertical borehole heat exchangers and four large heat pumps. The system serves a mix-use university building in the UK, providing both heating and cooling. Three-year monitoring data has been used and the three-year mean value of SPF2, corresponding to the energy performance of heat pumps and the ground loop circulating pump, has been reported to be 2.97. The overall system performance SPF4 has been reported to be 2.49. Two factors influencing the performance adversely are the hot water supply temperatures and the circulation pump energy demands. In a continuing study, Naicker and Rees (2019) have also analysed the performance of the borehole heat exchanger system using 38 months of monitored data. The results indicate that the ground heat exchange is highly related to the rejection of heat during the monitoring period and weather changes.

Bockelmann and Fisch (2019) have presented long-term performance measurements of geothermal heating and cooling systems of six different buildings in Germany. The study presents measurement results, seasonal performance analysis, operating experiences, as well as fault prevention strategies. The seasonal performance results are presented as SPF2 values, which present the performance of the compressor and circulating pump on the borehole side. The reported annual performance factors between different systems range between 2.5 and 6 in heating mode and between 4 to more than 100 in free and active cooling modes. The authors point out that continuous monitoring and quality assurance are of crucial importance, especially in the first years of operation.

Spitler and Gehlin (2019) have presented long-term performance measurement of a mixed-used 6300-m^2 student centre at Stockholm University in Sweden served by a GSHP system. The SPF values for both heating and cooling modes have been evaluated separately using the SEPEMO boundary scheme. Detailed uncertainties for performance parameters have also been presented. The measured SPF2 values, which correspond to the energy performance of the compressor and circulating pump on the borehole side, have been reported to be 3.7 ± 0.2 in heating mode and 27 ± 5 in free-cooling mode. The authors point out that one issue when calculating the whole system performance is the difficulty in separating the fan energy use between heating, cooling, and ventilation. It is suggested that the electrical energy consumption shall be divided based on pressure drop due to different system components in the ventilation system.

2.2 Ground heating and cooling system issues and solutions

Several studies, both experimental and field studies, have focused on practical issues and the performance improvement of geothermal heating and cooling systems. Many GSHP systems are operated mostly under partial load conditions, and the circulation pumps are operated at a constant speed, regardless of the load, which results in decreasing the system performance (Naicker and Rees, 2018). Shin and Cho (2018) proposed a variable flow rate control method based on the supply and return water temperature difference in a GSHP system. This solution has significant advantages for reducing the energy consumption of both the circulation pumps and the whole system. Malhotra et al. (2017) investigated ten ground source heat pump systems in the USA. The authors analyzed the reason for poor energy performance with daily performance values. The author showed that balancing the ground loads is the key to achieving the benefit of the ground source heat pump system. The paper even concluded that in order to eliminate the auxiliary heating and to optimize the energy yield from the heat pump system, the hot water temperature has to be carefully adjusted.

When building heating and cooling demands are not balanced, the thermal imbalance of the ground source results in a negative impact on the system performance. This issue has also been assessed and several possible solutions have been proposed. Zhai and Yang (2011) and Yu et al. (2011) presented a large-scale study on GSHP systems in an archive building in China. This system consists of two heat pumps each with a cooling capacity of 500 kW and 280 boreholes, each 80 m deep. Owing to the utilization of the condensation heat recovery technology, the heat rejected to the ground was reduced by 33 %, which provided a great advantage in keeping ground energy balanced. This study indicated that the GSHP systems have the potential to be successfully applied in the imbalanced ground energy conditions

without oversizing the ground system. Javed et al. (2019) showed that balancing the ground loads by changing the building envelop characteristics can help reduce the borehole system size and provide higher energy performance.

Integrating the ground source system with other energy sources is also an alternative method to improve system performance. Lazzarin et al. (2013) and Busato et al. (2013) performed a system performance analysis of a school with a ground source heat pump system working with a boiler and a solar energy system. The authors showed that a properly managed multi-source energy system shows better energy performance than each system working separately. Wemhoener et al. (2017) analyzed a ground source heat pump system working together with a solar energy system in a net-zero energy residential building in Switzerland. The study used a boundary scheme to analyze the system efficiency of a system with two energy sources. The results showed that a reasonably designed PV system can help compensate for the ground thermal imbalance and enhance the GSHP system performance.

2.3 Comparison of ground-source and air-source systems

Some field studies have focused on comparing the performance characteristics of ground source heating and cooling with air source systems. Michopoulos et al. (2007) analyzed a GSHP system with twenty-one boreholes, each 80-meter-deep, in Northern Greece. The paper compared the GSHP system energy performance with an air source heat pump system (ASHP) using three years of data. It was shown that higher efficiency and more stable working conditions of the GSHP system resulted in a 55 % higher performance than the ASHP system. Urchueguía et al. (2008) compared the ASHP and GSHP systems in a building in Spain. The paper showed that the ground source system is a more viable and energy-efficient option than the ASHP system. Furthermore, Hwang et al. (2009) performed the analysis for a ground source cooling system in Korea that has 24 boreholes, each 175 meters deep, and compared it with an ASHP system. It was shown that the COP of the GSHP unit could reach 8.3 and the COP of the GSHP system could reach 5.9, which were both significantly higher than those possible with the ASHP system to reach the same thermal comfort in the project. The author explained that it was because the condensing temperature in the GSHP was 10 ℃ lower than the ASHP system, which resulted in considerably lower energy consumption by the compressor.

3 Method

In this thesis, the performance of two ground source heating and cooling system has been evaluated. The first system is installed in a clubhouse with almost 240 m^2 floor area. The system comprises of a ground source heat pump system with a single 240 m deep borehole and two auxiliary electrical heaters. The long-term measurements have been carried out since 2010. For this study, three years of measurement data from January 2014 to December 2016 with 2 minutes of resolution have been used.

The second system is a large office building with an area of 65,265 m^2. The building has a direct ground cooling system, comprising of 144 boreholes, each 220-m deep. For this system, five-year monitoring data from January 2014 to August 2018 with 5 minutes resolution has been used.

For both case studies, the original data has been filtered for systematic and random errors, and converted to different time steps, such as hourly, monthly, and yearly. It is thus possible to perform hourly, monthly, and annual performance analysis. The analysis has been performed by calculating the seasonal performance factors (SPFs) for different system boundary schemes using the measurement data.

In this study, SPFs are calculated using two different approaches SEPEMO (SEasonal PErformance factor and MOnitoring for heat pump systems) boundary scheme and Annex52 boundary scheme. The two approaches use different boundaries to evaluate system performance factors. The SEPEMO boundary scheme was proposed by Nordman et al. (2012) to implement a common system evaluation for seasonal performance factors. Four different system boundary levels defined in the SEPEMO approach are shown in Table 1. The first level covers only the refrigeration cycle. The second boundary also includes the source-side pump. The third boundary additionally includes auxiliary heating. The fourth boundary includes all components in the system. This boundary scheme is quite popular in Europe and has been applied to 44 heat pump systems in six European countries. Most of these heat pump systems were installed in residential buildings, mostly single-family houses (Jeffrey and Gehlin, 2019).

Table 1: SEPEMO boundary scheme.

System Components	Boundaries			
	1	2	3	4
Source-side circulation pumps		√	√	√
Refrigeration Cycle	√	√	√	√
Distribution-side circulation pumps				√
Auxiliary heating			√	√

Recently, the IEA-HPT Annex 52 has been initiated to collect long-term measurement data of ground source heating and cooling systems and to characterize the GSHP system performances. A new system boundary scheme has been proposed within the Annex52 group.

The new scheme accounts for various complexities and subsystems present in larger and more complex GSHP systems (Gehlin and Spitler, 2020). As shown in Table 2, there are six main system boundary levels defined in Annex52 boundary scheme. Additionally, the '+' superscript is used for auxiliary heating or cooling within a boundary.

Table 2: ANNEX 52 boundary scheme.

System Components	Boundaries											
	0	0+	1	1+	2	2+	3	3+	4	4+	5	5+
Source-side circulation pumps	√	√			√	√	√	√	√	√	√	√
Refrigeration cycle			√	√	√	√	√	√	√	√	√	√
Buffer tank and circulation pumps between heat pump and buffer tank							√	√	√	√	√	√
Circulation pumps between buffer tank and distribution system									√	√	√	√
Distribution system											√	√
Auxiliary heating		√		√		√		√		√		√

The first case study has been evaluated using both SEPEMO and Annex 52 boundary schemes. For the second case study, only the Annex 52 boundary scheme has been applied. For both systems, SPFs have been calculated for the monthly and yearly periods. The results of SPFs lead to better insight to compare the GSHP system performance, which is mainly influenced by the set system boundaries.

Moreover, an uncertainty analysis has been carried out for each case study. The measurement uncertainties of the sensors have been used to determine uncertainties in the thermal energy, electrical energy, and monthly and yearly SPFs. More detailed information is presented in each case study.

4 Case study 1

This chapter describes the first case study building and its GSHP system, explains the measurement setup, and presents the GSHP system performance.

4.1 System description

The first case study investigated in this thesis is a clubhouse located in Sisjön (near Gothenburg), Sweden. The clubhouse was built in 2004 and has an area of around 240 m². The clubhouse is used as a service space for outdoor orienteering activities. It has a multi-purpose community room, and locker rooms with hot showers, and saunas. Figure 1 shows the picture and layout of the clubhouse. A shallow geothermal heat pump provides heating and DHW to the clubhouse. The clubhouse has a high domestic hot water demand because of the changing room showers. The installed GSHP system has a total capacity of 11 kW. The ground heat exchanger is a groundwater-filled borehole as common in Sweden (Spitler et al., 2016), drilled to a depth of 230 m, and fitted with a single U-tube filled with an ethanol/water mixture.

(a)

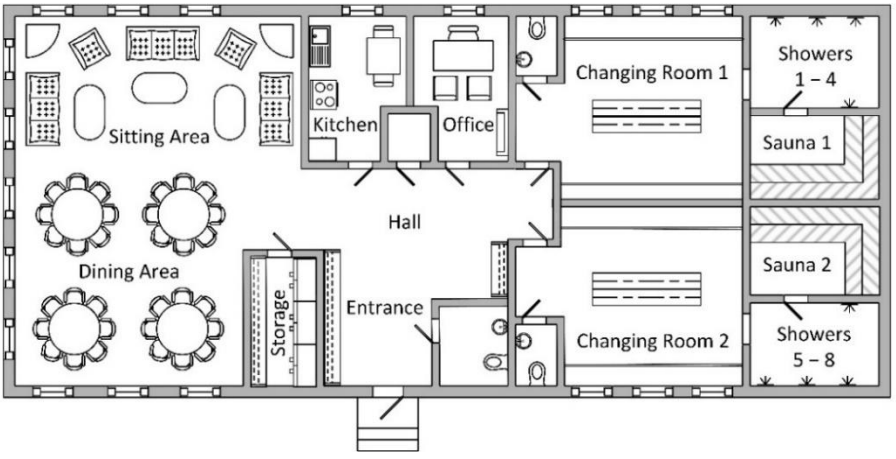

(b)

Figure 1: Sisjön clubhouse (a) picture and (b) layout.

A schematic of the clubhouse space heating and DHW system is shown in Figure 2. The heat pump unit consists of a 5 kW compressor, a 6 kW auxiliary heater, and two circulation pumps. The GSHP system in addition includes two 500-liters buffer tanks to cover the DHW demands of the clubhouse. A legionella protection system is incorporated into the heat pump system. This protection system runs once a week and raises the water temperature to 60 °C. The heat pump also has a built-in intelligent control system that calculates the heating demand of the clubhouse based on the outdoor temperature. A low-temperature heating supply system is used in the clubhouse. Heat distribution inside the building is provided by radiators using a supply water temperature of approximately 30–40 °C. The low-temperature heating system is aimed at providing higher energy-efficiency than the high-temperature heating system. The DHW is stored and distributed through the two 500-liters storage tanks. The first tank supplies the water to the second tank. An electric resistance heater of 3 kW is installed in the second tank. The DHW temperature is maintained at approximately 55–60 °C by this electric heater. The heat pump prioritizes DHW production over space heating. The hot water produced by the heat pump is either passed through to the space heating system or the DHW tanks depending on a reversing valve which changes position when the DHW temperature has reached a certain level.

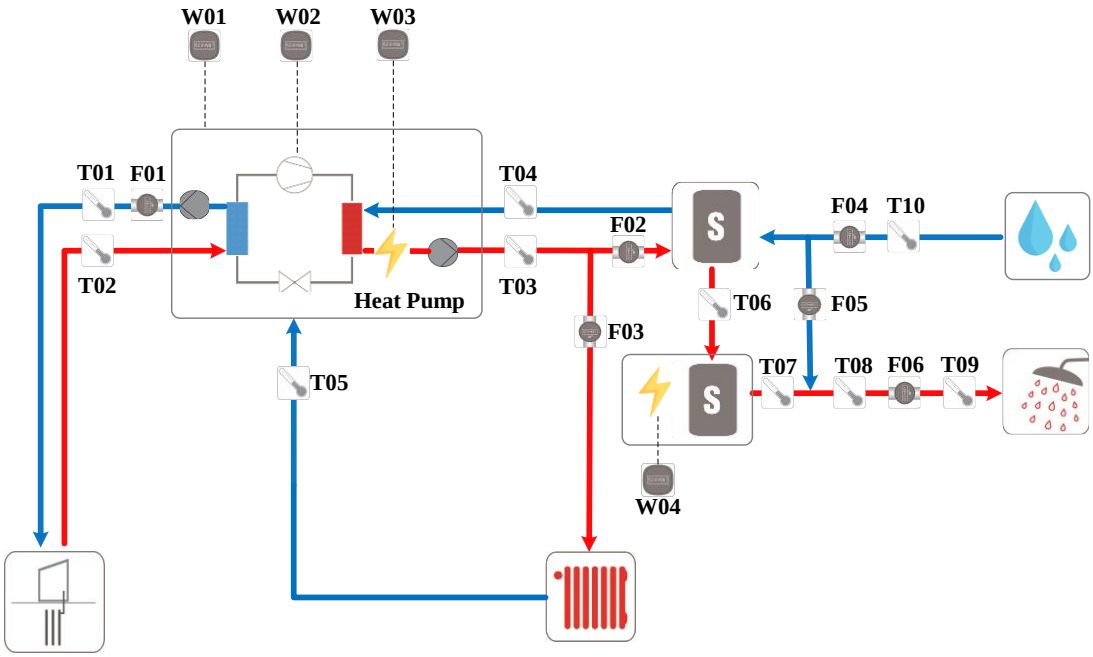

Figure 2: Schematic of the GSHP system of the Sisjön clubhouse.[1]

4.2 Measurements

High-frequency measurement data from the clubhouse were undertaken to characterize the actual performance of the GSHP system. Measurements of temperature, flow, and electrical energy consumption data with a measuring interval of 2 minutes was collected for the period

[1] Pictograms in drawing used with permission from TU Braunschweig IGS.

of January 1, 2014, to December 31, 2016. Besides, hourly outdoor air temperatures from Landvetter, Gothenburg (SMHI 2020) were obtained to calculate the energy signature of the building.

The measurement setup of the clubhouse used for the collection of measurement data comprised of ten temperature and six flow sensors installed in the borehole loop, the heat pump circuit, and the building distribution system. There were also four electrical energy meters installed for measuring the electrical energy consumption of the compressor, two auxiliary heaters, and the heat pump (Figure 2). Temperature difference measurements were performed using paired PT-100 temperature sensors with ±0.1 K absolute uncertainty to ensure high accuracy. A vortex flow sensor (F01) with ±6 % fractional uncertainty was used for borehole flow measurements. Vortex flow sensors (F02–F05) with ±3 % fractional uncertainty were used for water flow measurements. In addition, a pulse meter (F06) was also used to measure the domestic water flow supplied to the clubhouse. The electrical energy meters had an accuracy of ±1 %. The space heating energy and DHW energy delivered by the heat pump were calculated using the measured flow rate and the measured ΔT. The electrical energy consumption of the two circulation pumps was not metered directly. However, as the total electrical energy consumption of the heat pump was measured, the energy consumed by the pumps and the heat pump control system could be calculated together by subtracting the energy consumed by the heat pump auxiliary heater and the compressor from the total energy consumed by the heat pump. However, for the purpose of the analysis, it was necessary to separate the energies used by the two circulation pumps. Hence, a separate set of measurements was made to estimate the electrical power (kW) used by the source-side circulation pump. The electric meter P01, measuring the heat pump unit that includes a compressor, two circulation pumps, auxiliary heater, and the control system, was used to determine the power consumption of the control system using the periods when there were no DHW or space heating demands and when the pumps were not running. Similarly, the power input to both circulation pumps was estimated considering periods over which only one pump was operating. The power input of the pumps and the control system was integrated over actual run times to determine their respective energy consumptions.

The long-term monitoring data was compiled and debugged to get rid of systematic and random errors. In the first step, each sensor measurement was corrected using the calibration data, and the raw data were corrected using a Matlab program. The flow values, originally measured in volts, were converted to litres/minute. Similarly, the energy values, originally measured as pulses, were converted to kWh (250 pulses corresponded to 1 kWh). The electrical power inputs to the heat pump, electric heaters, and compressor were taken from the electrical energy meters. Sometimes there were small breaks in some measurements. In that case, a polynomial regression algorithm was used to fill the gaps using Matlab. Furthermore, a regressive test on the energy model was made to make sure all the filled data was reliable. Finally, all the values were recuperated in the text format.

Different data handling time steps were used depending on the requirement of the data analysis. The original two-minutes time step was used for incorporating data corrections and sensor calibrations. The hourly average data was used for detailed analysis, especially for analyzing sensitivities of results to variations in operating conditions. The monthly and yearly time steps were used for general analysis of the trends and for calculating the overall system performances.

In September 2015, the speed of the demand-side circulation pump was increased slightly. Moreover, in August 2015, the setpoint temperature of the auxiliary heater installed in the second tank was also changed. These modifications made it possible to analyze how changes in energy consumption of different system components influence the performance. As noted by Bockelmann and Fisch (2019), such measurements can contribute to gain insight into how various system components and control systems affect the overall performance. It can also lead to identifying best solutions, highlighting design and monitoring issues that cause poor performance, and offering recommendations that may contribute to improving the system design and operation.

4.3 System boundaries

SEPEMO project (Nordman et al., 2012) presented a benchmarking method for evaluating the seasonal performance of heat pump systems, where the impact of the auxiliary components is incorporated into the evaluation. As noted by Spitler and Gehlin (2019), the SEPEMO method is mainly focused on small-sized heat pump system for heating and/or cooling. The clubhouse system is also a fairly small GSHP system with one borehole and a heat pump. All SEPEMO boundaries can be applied to the clubhouse ground source heat pump system for calculating different seasonal performance factors. Figure 3 presents the SEPEMO system boundaries applied to the clubhouse system.

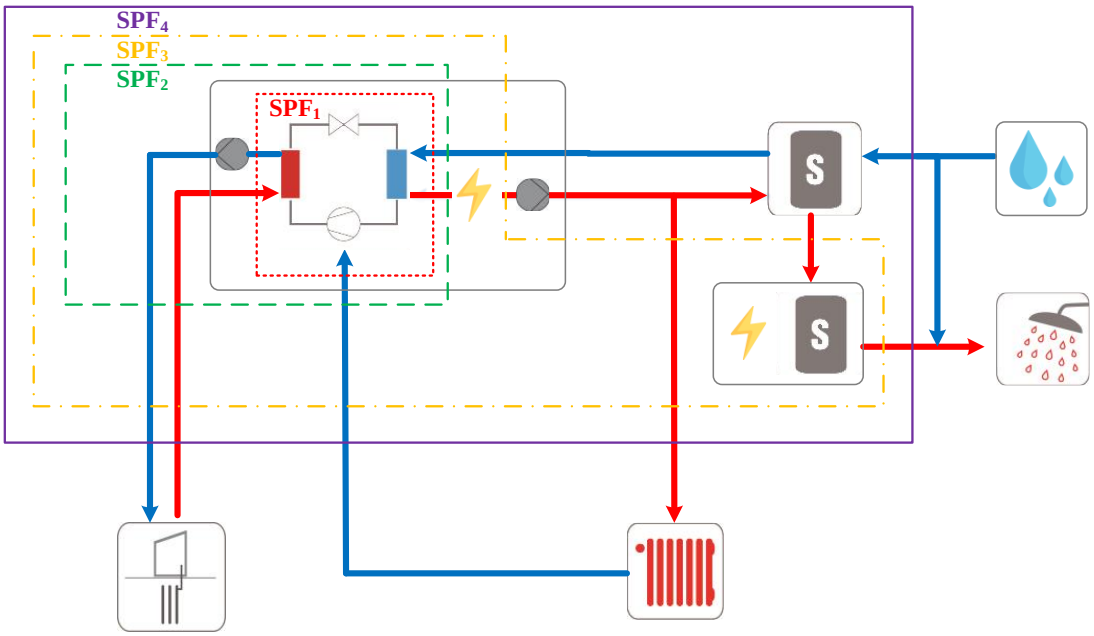

Figure 3: SEPEMO boundaries applied to the clubhouse system.[2]

[2] Pictograms in drawing used with permission from TU Braunschweig IGS.

Table 3: SPF formulas for the SEPEMO boundary scheme.

$SPF_1 = \frac{Q_r}{W_c}$
$SPF_2 = \frac{Q_r}{W_{p,s} + W_c}$
$SPF_3 = \frac{Q_r + Q_{ah}}{W_{p,s} + W_c + W_{ah}}$
$SPF_4 = \frac{Q_r + Q_{ah}}{W_{p,s} + W_c + W_{p,l} + W_{ah}}$

As Table 3 shows, SPF1 measures the performance of the refrigeration cycle itself, and only the compressor electrical energy consumption is considered. SPF2 also considers the energy consumption of the source-side pump. It may be used for comparing the GSHP system with other technologies. SPF3 takes energy consumption of auxiliary heating into account and measures the performance of the system without the distribution system. SPF4 also includes the energy consumption of the distribution pumps and gives the overall performance of the whole GSHP system.

The IEA-HPT Annex 52 has developed a new boundary scheme based on the SEPEMO scheme. The Annex 52 boundary scheme enables a more detailed performance comparison between system components. Figure 4 (a) and (b) show the Annex 52 system boundaries applied to the clubhouse system. The boundary 0 only includes the borehole exchanger and the source-side pump. Boundary 1 measures the refrigeration cycle performance. Boundary 2 takes the energy consumption of the source pump and the compressor into account. Boundary 3 also includes the energy consumption of the load-side pump. For the Annex 52 scheme, the '+' superscript indicates auxiliary heating/cooling within the boundary. As shown in Figure 4 (b), boundary 1+ includes the energy consumption of compressor and heat pump auxiliary heater. Boundary 2+ includes the source-side pump, compressor, and heat pump auxiliary heater. Boundary 3+ includes the energy consumption of the whole circulation system of the clubhouse, including the auxiliary electric heater in the tank. Table 4 shows the formulas used for calculating SPFs according to the Annex 52 boundary scheme.

Comparing SEPEMO and Annex 52 boundary schemes, SPF1 and SPF2 in the SEPEMO scheme correspond respectively to SPF1 and SPF2 in the Annex 52 scheme. The SPF3 in the SEPEMO scheme, which includes ground source circulation pump, heat pump unit, and two auxiliary heaters in the system, corresponds to SPF 2+ in the Annex 52 scheme. However, in this system, SPF 2+ in the Annex 52 scheme does not include the auxiliary heater in the tank.

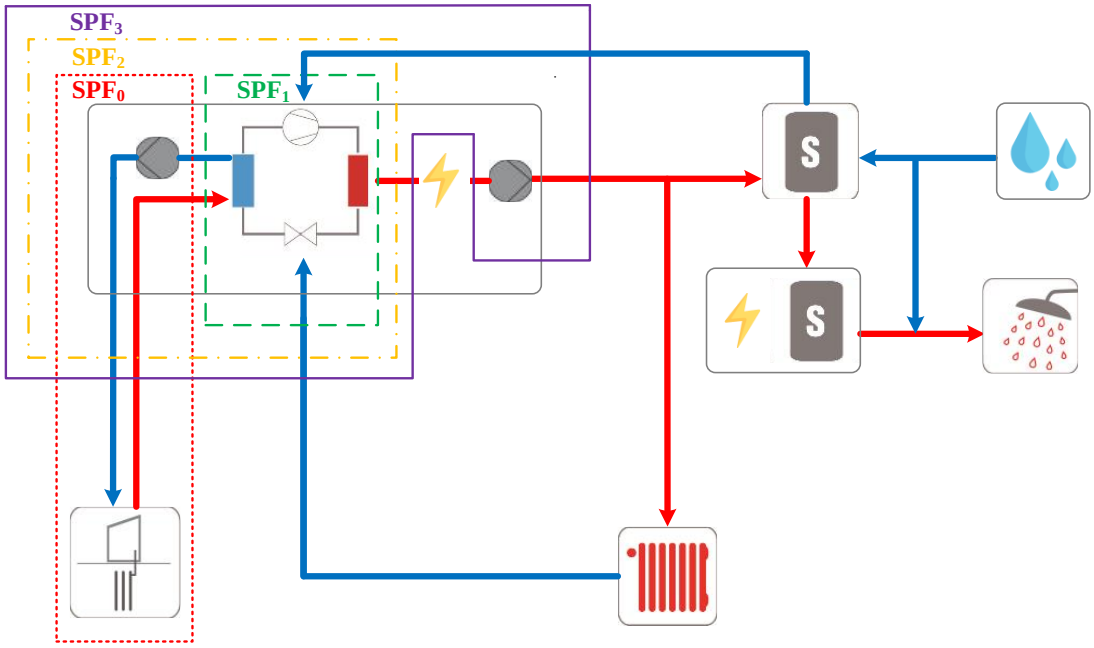

(a)

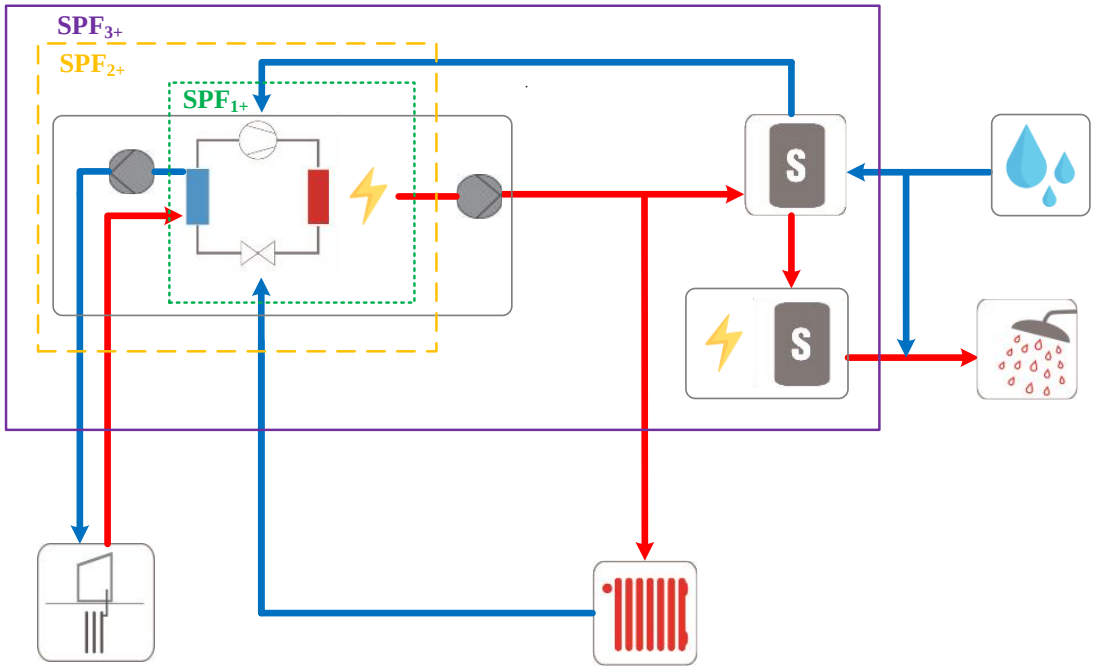

(b)

Figure 4: Annex 52 boundary scheme applied to the clubhouse system.[3]

[3] Pictograms in drawing used with permission from TU Braunschweig IGS.

Table 4: SPF formulations for Annex 52 boundary scheme.

$SPF_0 = \frac{Q_{ghe}}{W_{p,s}}$
$SPF_1 = \frac{Q_r}{W_c}$
$SPF_{1+} = \frac{Q_r + Q_{ah}}{W_c + W_{ah}}$
$SPF_2 = \frac{Q_r}{W_{p,s} + W_c}$
$SPF_{2+} = \frac{Q_r + Q_{ah}}{W_{p,s} + W_c + W_{ah}}$
$SPF_3 = \frac{Q_r}{W_{p,s} + W_c + W_{p,l}}$
$SPF_{3+} = \frac{Q_r + Q_{ah}}{W_{p,s} + W_c + W_{p,l} + W_{ah}}$

4.4 Uncertainty analysis

The uncertainties in delivered thermal energy, consumed electrical energy, and calculated SPFs have been estimated to determine the reliability of results. The approach described by Spitler and Gehlin. (2019) has been used. The uncertainties have been calculated for the monthly and yearly results.

4.4.1 Thermal energy

The thermal energy delivered by the ground and the heat pump is calculated based on the temperature difference between supply and return fluids and the volume flow. The paired temperature sensors used in the clubhouse had an absolute uncertainty of 0.1 K, while the flow sensors had fractional uncertainties of 3 and 6 % for water and brine flows, respectively. Although the specific heat and density also varied with temperature, the uncertainties in these values were relatively small, and thus ignored. The individual uncertainties are expressed as Equations 1 to 4.

$$E_{\Delta T} = \pm 0.1\ K \tag{1}$$

$$e_{\Delta T} = \pm \frac{0.1}{\Delta T} \tag{2}$$

$$e_{\dot{V},w} = \pm 3\ \% \tag{3}$$

$$e_{\dot{V},b} = \pm 6\ \% \tag{4}$$

The absolute uncertainties are expressed as upper-case '*E*' and the fractional uncertainties are expressed as lower-case '*e*'. Since the temperature and flow uncertainties are mutually independent, the uncertainties in the thermal energy transfer rate can be calculated using Equation 5.

$$e_q = \sqrt{{e_{\Delta T}}^2 + {e_{\dot{V}}}^2} \tag{5}$$

The fractional uncertainties of thermal energy transfer rate can be converted to absolute uncertainties and then converted to absolute uncertainties of thermal energy with Equation 6 and 7.

$$E_q = e_q * q \tag{6}$$

$$E_Q = E_q * \Delta t \tag{7}$$

The monthly and annual thermal energy uncertainties are determined by aggregating the absolute uncertainties in thermal energy in different time steps using Equations 8, and 9.

$$E_{Q,n} = \sum_{i=1}^{n} E_{Q,i} \tag{8}$$

$$e_{Q,n} = \frac{E_{Q,n}}{\sum_{i=1}^{n} Q_i} \tag{9}$$

4.4.2 Electrical energy use

Four electrical energy meters have been used to measure the electrical energy input of different heat pump components. The electrical energy meter used in the clubhouse has uncertainties of ±1 %. For each SPF boundary, the uncertainty of each component is considered. For example, the uncertainty of electrical energy consumed in SEPEMO boundary 4 can be determined using Equation 10.

$$E_W = \sqrt{{E_{p,s}}^2 + {E_c}^2 + {E_{p,l}}^2 + {E_{ah}}^2} \tag{10}$$

The monthly and yearly absolute uncertainties in energy consumption are calculated using Equation 11 and then converted into fractional uncertainties with Equation 12.

$$E_{W,\,n} = \sum_{i=1}^{n} E_{W,\,\mathrm{i}} \tag{11}$$

$$e_{W,n} = \frac{E_{W,n}}{\sum_{i=1}^{n} W_i} \tag{12}$$

4.4.3 Seasonal performance

Once the uncertainties in thermal energy use and electrical energy use have been calculated, the uncertainties in the seasonal performance factors can be determined. The uncertainties in thermal energy and electrical energy use can be added in quadrature using Equation 13 to determine the uncertainties in SPF values.

$$e_{SPF,n} = \sqrt{{e_{Q,n}}^2 + {e_{W,\,n}}^2} \tag{13}$$

4.5 Results

This section presents the results of measured data and energy performance analysis of the clubhouse GSHP system for three years.

4.5.1 Ground heat exchange and load characteristics

The ground is a good source of heating for heat pump systems as the temperature of the ground is fairly constant over the year. The daily mean supply temperatures from the clubhouse borehole system for the measurement period are shown in Figure 5 along with the daily mean outdoor air temperatures. As seen from the figure, the daily mean borehole supply temperatures during the evaluation period remained quite stable and varied in a rather narrow range. The supply temperatures were slightly higher in summer than in winter. The relatively high supply fluid temperatures indicate that even after several years of heat extraction, the ground system of the clubhouse is capable of providing fluid at high extraction temperatures to the heat pump. Also, it can be observed that the 2015 – 2016 winter was colder than other years which might have caused a higher heating energy demand in 2016.

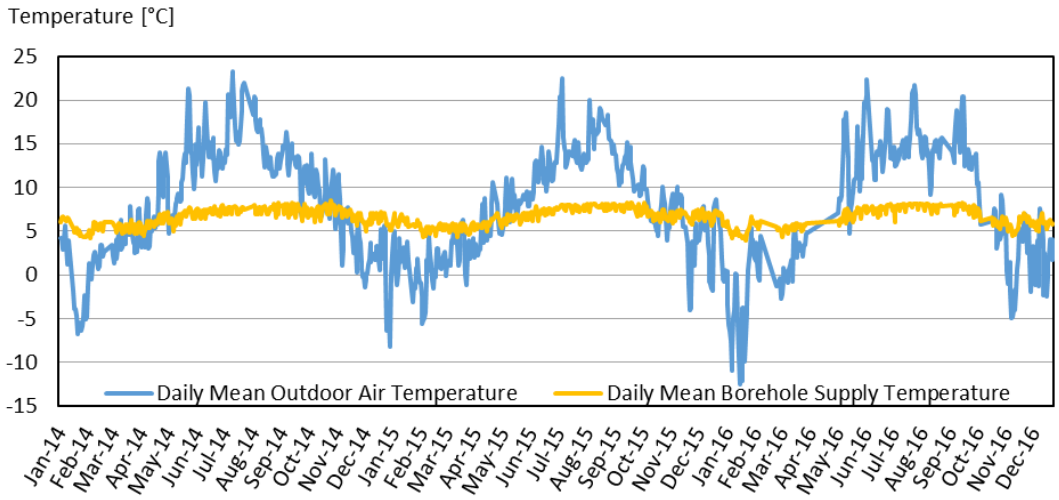

Figure 5: Daily mean borehole supply and outdoor air temperatures.

In order to study the borehole performance further, the specific borehole extraction rate is presented in Figure 6 against the outdoor air temperature. It can be noticed that the peak specific heat extract rates are around 15 W/m. The common range for this value is between 50 and 70 W/m (VDI 4640, 2001). This suggests that the borehole system in the clubhouse has been oversized.

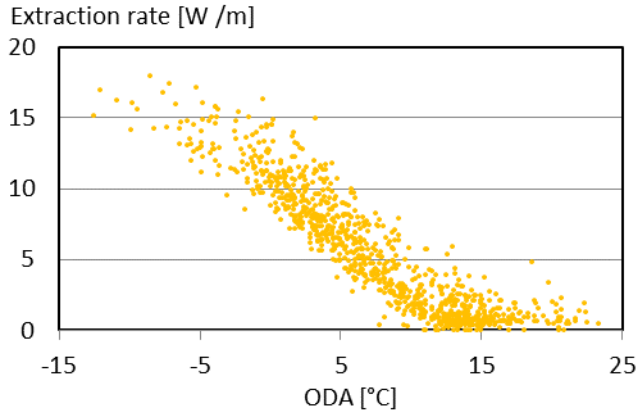

Figure 6: Specific borehole heat extraction rates.

As mentioned earlier, the clubhouse GSHP system has a nominal heating capacity of 11 kW, which comprises of a 5 kW compressor and a 6 kW auxiliary heater built in the heat pump. The heat pump auxiliary heater is only operated for the provision of DHW. The heat pump is controlled to match the required loads by switching on or off the compressor. Figure 7 presents the heat pump delivered energy per hour for both the DHW and space heating systems as a function of the outdoor air temperature. The values shown in the figure are calculated based on the average hourly data. The DHW load is very modest and is nearly constant at less than 1 kWh/h for the entire outdoor air temperature range of -10 ℃ to 21 ℃.

However, the space heating load system has a different trend. The space heating loads decrease with increasing outdoor air temperatures.

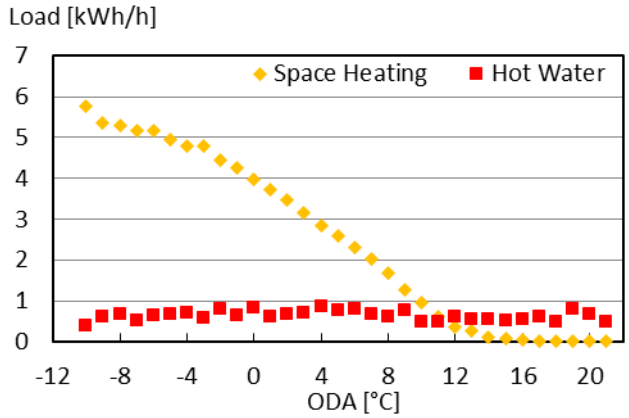

Figure 7: Heating load for DHW and space heating.

4.5.2 Energy performance

The heat pump delivered energy can be separated into two parts, the energy delivered for space heating and the energy delivered for DHW. The measured supply and return water temperatures in the DHW and space heating modes are illustrated in Figure 8. As seen from Figure 8 (a), the supply water temperatures in the DHW mode vary between 55 ℃ to 62 ℃. On the other hand, as seen in Figure 8 (a), the supply temperatures are outdoor temperature-compensated. The supply temperatures reach 40 ℃ in the coldest months, with the return temperatures around 32 ℃.

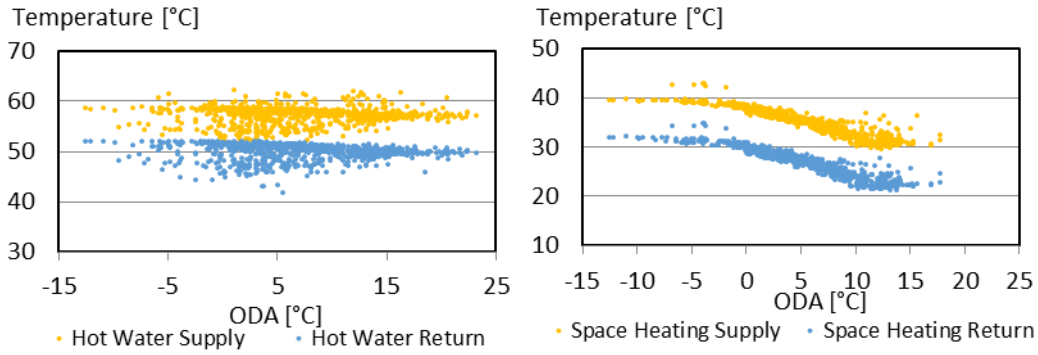

Figure 8: Supply and return temperatures (a) DHW and (b) space heating for 2014-2016.

The measured monthly space heating and hot water loads for the clubhouse for the three years of measurement period are shown in Figure 9. As can be inferred from this figure, the monthly energy supplied to the DHW system remains fairly constant throughout the measurement period. For the space heating system, the monthly delivered energy varies between 10 kWh to 3500 kWh, with the peak values occurring between January and March. Overall, the energy demand for the space heating system constitutes a major part of the total energy demand.

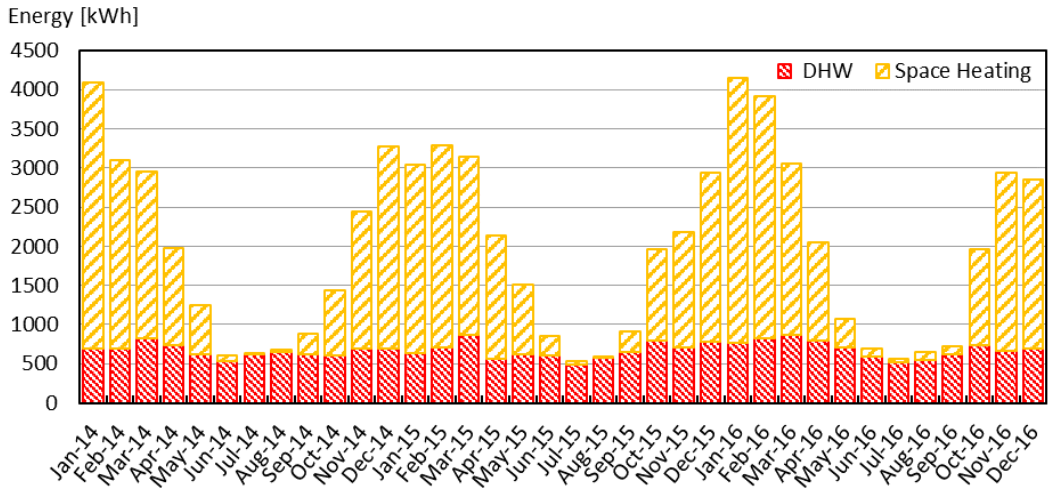

Figure 9: Measured monthly heating and hot water loads.

In the scope of this thesis, the electrical energy consumed by different system components has also been calculated and analyzed for all months from 2014 to 2016. Figure 10 shows the monthly electrical energy consumption of different system components, including the compressor, electric heater inside the heat pump, electric heater in the tank, and the circulation pumps. It can be seen that most energy is consumed by the compressor. The monthly energy consumed by the tank electric heater is higher than the energy consumed by the circulation pumps. The auxiliary heater in the heat pump has nearly constant electrical energy consumption throughout the measurement period, except in January 2014, when the energy consumed by the heat pump electric heater was even higher than the energy consumed by the compressor. It was because the compressor was broken at that time, and the heat pump electric heater was used for producing space heating and DHW. It can be noticed that the energy consumed by the clubhouse GSHP system has a seasonal dependence. In winter months, the total electrical energy consumption of the GSHP system components is significantly higher than the electrical energy consumption in the summer months.

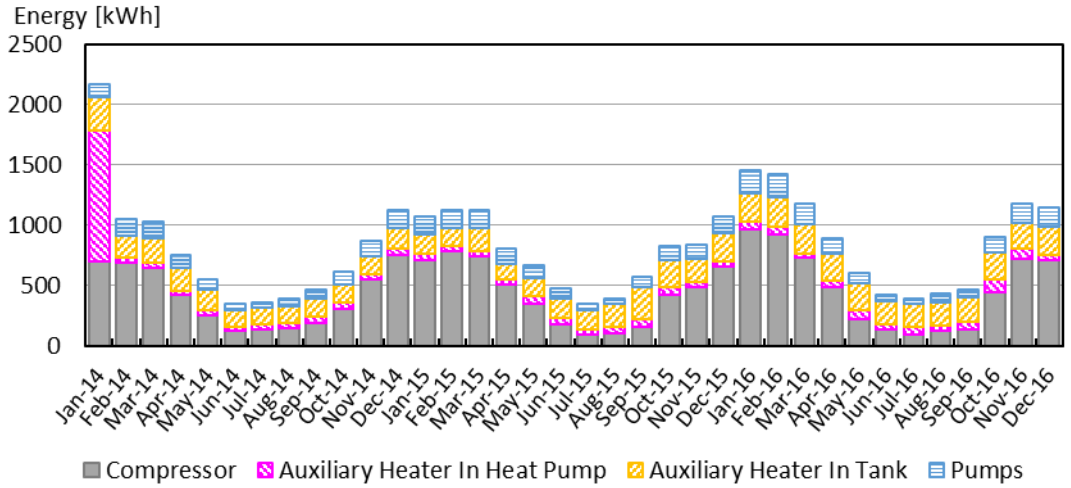

Figure 10: Energy consumption of different GSHP components.

To analyze the energy consumption more clearly, the percentage share of energy consumed by different system components has been evaluated. Figure 11 presents the electrical energy consumption of different system components in percentage values. In summer, the compressor generally uses less than 40 % of the total consumed energy, whereas in winter the compressor energy use is typically higher than 60 %. There is, however, an opposite trend of the energy consumption for the tank electric heater. In summer the tank electric heater consumes approximately 40 % of the total energy, while in winter it consumes around 15 % of the total energy. The percentage share of the electrical energy consumed by the heat pump electric heater is also higher in the summer months. The circulation pumps have a fairly similar percentage share of the electrical energy consumption throughout the measurement period. Based on these results, it can be anticipated the SPF values would be lower in summer due to the high percentage share of auxiliary components and would be higher in winter due to the lower percentage share of auxiliary components.

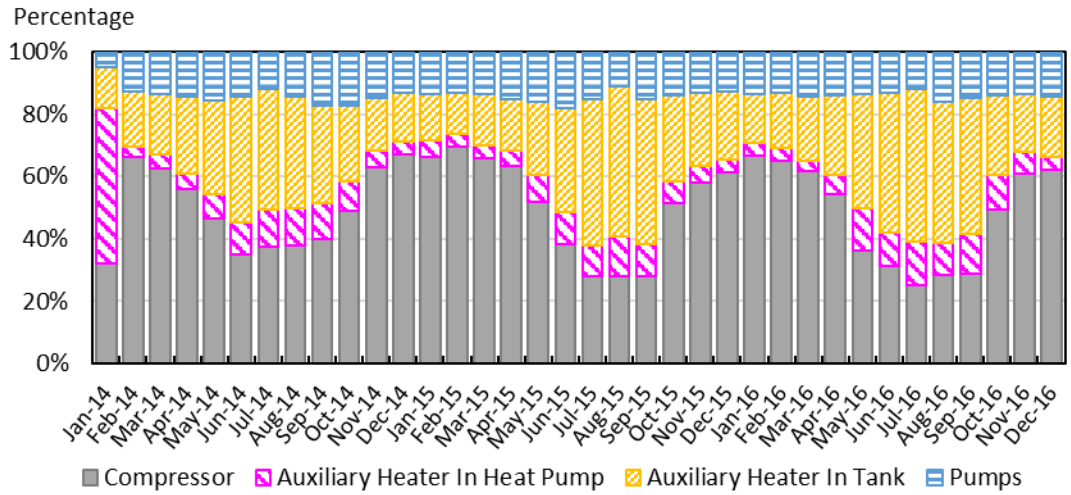

Figure 11: Percentage of energy consumption of different system components.

4.5.3 Seasonal performance factors

Based on the thermal energy supplied by the clubhouse system and electrical energy consumed by different GSHP system components, the monthly and annual performance factors have been calculated using SEPEMO and Annex 52 boundary schemes.

Figure 12 presents the annual SPF values for the four system boundaries of the SEPEMO scheme. The uncertainty range for all SPF values is also shown. The system performance in 2016 was comparatively lower. This can be attributed to the speed increase of the distribution-side circulation pump and the higher thermostat setpoint-temperature of the tank auxiliary heater. The detailed impact of these changes has been analyzed in the following. Besides, the SPF values decrease as the system boundaries are extended. The biggest drop occurs between SPF2 and SPF3 due to the high energy consumption of auxiliary heaters.

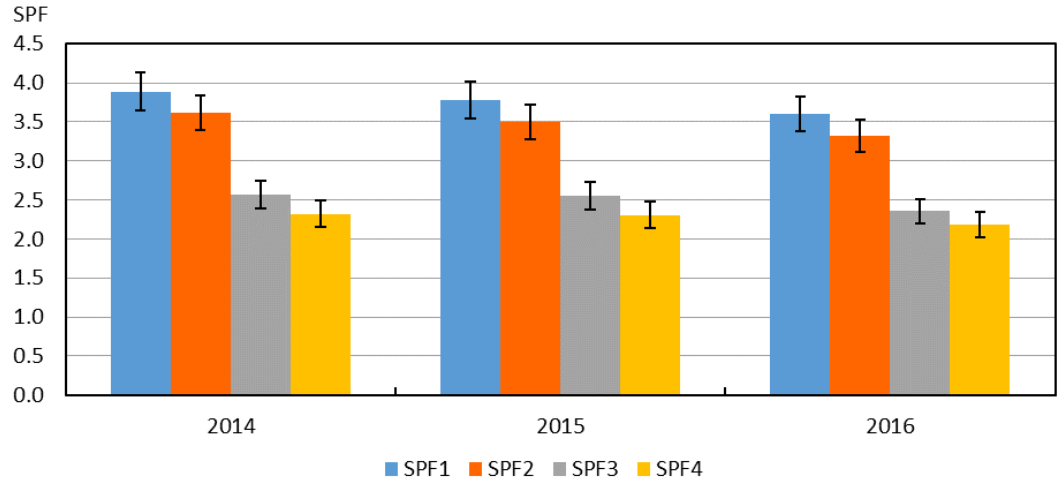

Figure 12: Annual SPFs based on the SEPEMO boundary scheme.

The monthly performance factors for the four SEPEMPO system boundaries are presented in Figure 13 for the whole measurement period. The uncertainties in SPF1 and SPF4 values are also shown. The SPF1 values vary between around 3.3 ± 0.2 in summer to up to 4.2 ± 0.26 in winter. Higher SPF1 values corresponded to periods when the heat pump operated more in the space heating mode than the DHW mode. The SPF2 values are slightly lower than SPF1 values. The SPF3 values, on the other hand, are significantly lower than the SPF2 values. The large gap between the SPF2 and SPF3 values indicates that the auxiliary heating contributes significantly towards the decrease in the performance of the clubhouse GSHP system. Finally, the SPF4 values vary between 2.9 ± 0.21 in winter and 1.5 ± 0.1 in summer. The monthly SPF values indicate that the performance of the system is season dependent. The performance is higher in winter than in summer. It is because the compressor has the highest percentage energy consumption in winter months, whereas the tank electric heater has the highest energy consumption in the summer months. The SPF3 and SPF4 values are quite low for January 2014. It is due to the compressor breakdown, which forced the heat pump electric heater to operate as the main heat provider.

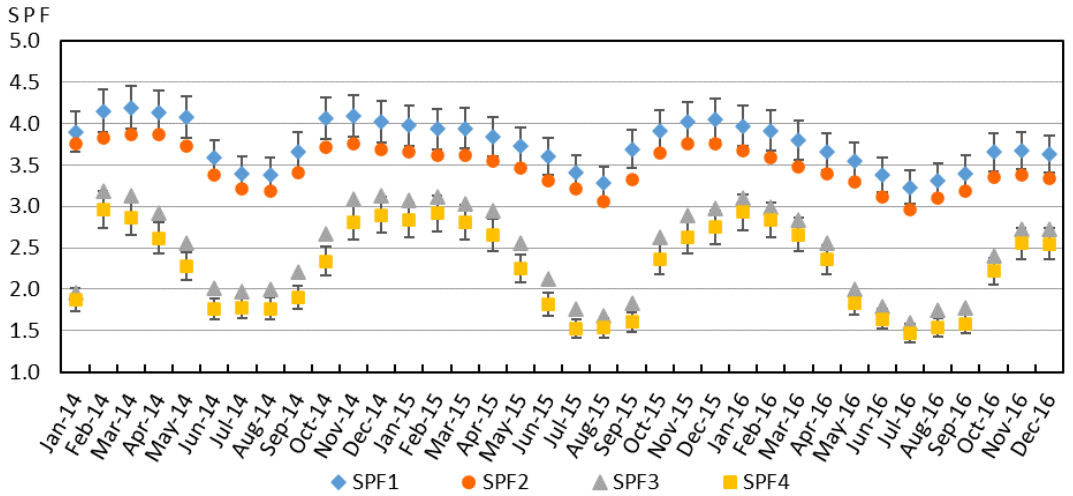

Figure 13: Monthly SPFs based on the SEPEMO boundary scheme.

Figure 14 presents the annual SPFs of the clubhouse system for the Annex 52 scheme. The figure also presents the uncertainty range for each SPF. The SPF values are presented using a logarithmic scale on the y-axis. The SPF4 and SPF5 values are not explicitly shown as they are equal to SPF3 values for the clubhouse system. The annual values of SPF0 for the three years of measurement period are between 33.8 ± 2.0 and 34.9 ± 2.1. The general trend of SPF is similar to those observed for the SEPEMO boundary scheme. The SPF1 values range between 3.2 ± 0.2 and 3.6 ± 0.23. It is rather low in 2014 due to the compressor failure, which forced the heat pump electric heater to provide space heating and DHW for several weeks. The effects of auxiliary heating in the buffer tank are also significant. For example, the annual SPF3 and SPF3+ values for the measurement period are between 2.8 ± 0.2 and 3.0 ± 0.21, and between 2.2 ± 0.16 and 2.5 ± 0.19, respectively. The large drop in values from SPF3 to SPF3+ illustrates the influence of both the heat pump and the water tank electric heaters on the system performance. Another notable point is that the SPF values in 2016 are generally lower than the values in 2014 and 2015. This is due to changes in pump speed and thermostat setpoint of heat pump auxiliary heater in the autumn of 2015.

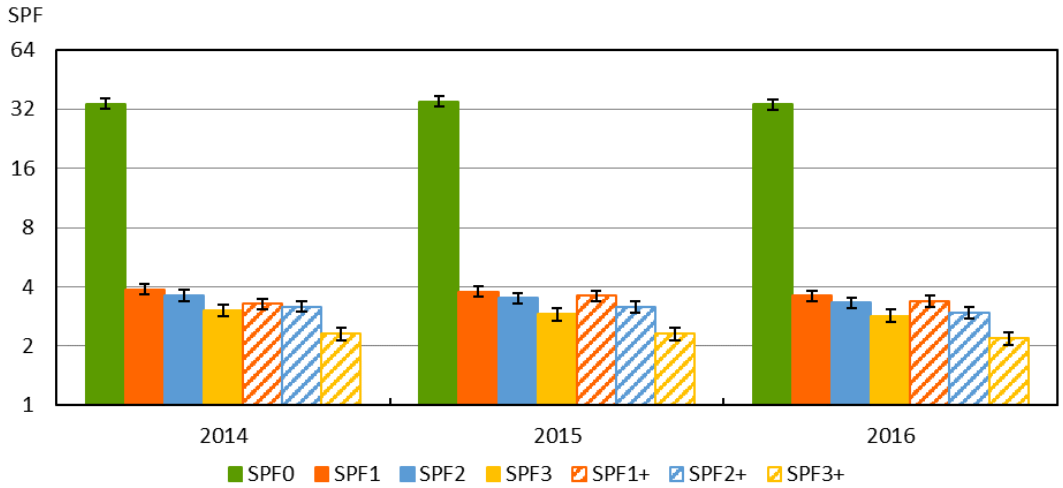

Figure 14: Annual SPFs based on Annex 52 boundary scheme.

Figures 15 (a), (b), and (c) present the monthly SPF values for the Annex 52 boundary scheme. The uncertainty ranges of SPF1, SPF1+, SPF3, and SPF3+ are also shown. The monthly SPF0 values, indicating the efficiency of the borehole system, range between 29 ± 1.7 and 40 ± 2.4 over the three years measurement period. The SPF1 values in Annex 52 boundary scheme are the same as SPF1 values in the SEPEMO boundary scheme. The monthly values of SPF2 and SPF3 vary between 2.9 ± 0.19 and 3.9 ± 0.23 and between 2.2 ± 0.13 and 3.5 ± 0.22, respectively. The SPF2 and SPF3, respectively, show the effect of borehole-side and distribution-side circulation pumps on the performance. It can be seen that the impact of distribution-side circulation pumps is more pronounced than the borehole-side circulation pump. The SPF1+, SPF2+, and SPF3+ values show the effect of auxiliary heating within their boundaries. The monthly values of SPF1+ and SPF2+ are slightly lower than the corresponding values of SPF1 and SPF2. The SPF3+ values, presenting the overall monthly performance of the clubhouse system, are between 1.5 ± 0.11 and 3.1 ± 0.23. The values of SPF1+, SPF2+, and SPF3+ values for January 2014 are significantly low because the compressor was broken and the electrical heater worked instead. The difference between SPF1 and SPF1+ values is higher in summer than in winter as the heat pump auxiliary heater

has a higher percentage of energy consumption in summer. It can also be noticed that system performance is largely affected by the tank auxiliary heater. The gap between SPF3 and SPF3+ is larger than the gap between SPF1 and SPF1+ indicating that the energy use of the tank auxiliary heater contributes more to the decrease in the efficiency of the system than the heat pump electric heater. Overall, the huge difference between the SPF1 and SPF3+ values indicate that pumps and auxiliary heaters in the system play a critical role in decreasing the system performance. Similar to the annual SPFs, the monthly SPF values are lower for 2016 due to the increased energy consumption of pumps and electric heating following the changes in operating conditions in autumn 2015.

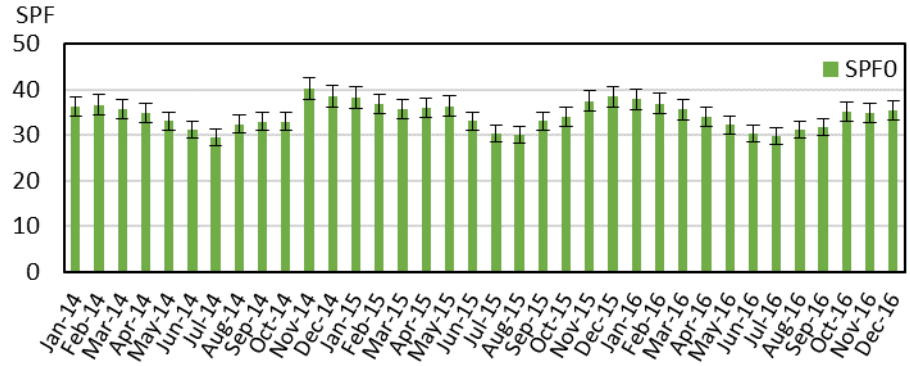

(a)

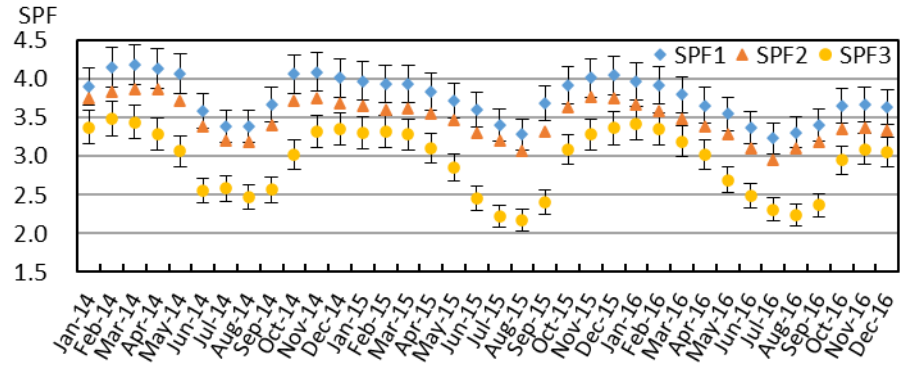

(b)

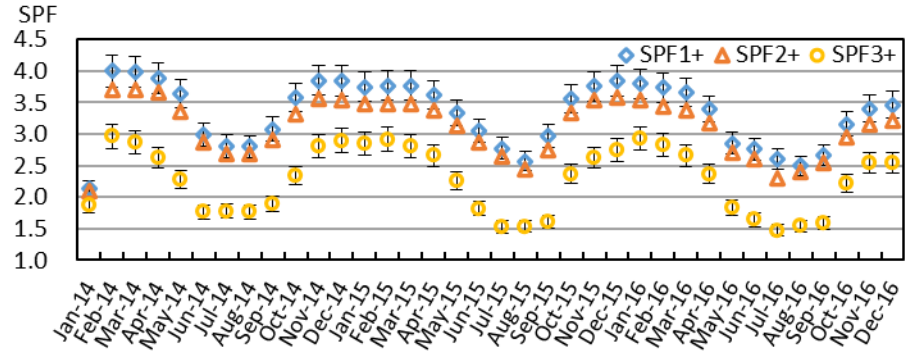

(c)

Figure 15: Monthly SPFs based on the Annex 52 boundary scheme.

4.5.4 Further analysis

The tank auxiliary heater has been shown to have high electrical energy consumption and to have a large impact on system performance. To fully understand the impact of the tank auxiliary heater, the SPF3+ values for the DHW system are compared with a hypothetical case of SPF3+ values not accounting for the energy use of the tank auxiliary heater. Figure 16 presents the SPF3+ values for the DHW system in 2015 for these two cases. The figure shows that the energy use of the tank auxiliary heater decreased the SPF values by around 1. This suggests that the tank auxiliary heater is one of the most critical components influencing the system performance.

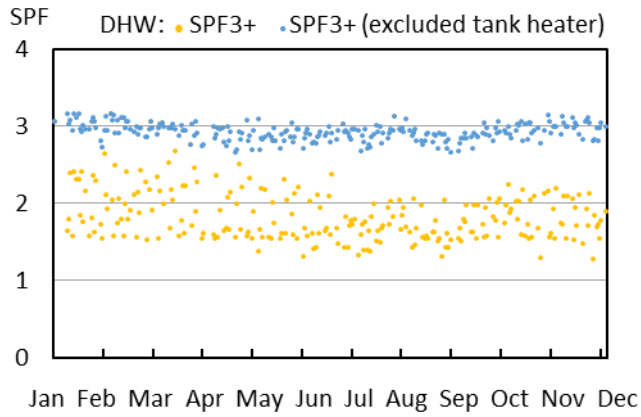

Figure 16: SPF3+ values of the DHW system with and without tank auxiliary heater in 2015.

As mentioned before in section 4.1, the distribution-side pump speed was increased in September 2015. The effect of this change has been investigated with Annex 52 boundary scheme for both DHW and space heating systems. The hourly SPF3 values of Annex 52 boundary scheme for the DHW system before and after pump speed change are shown in Figure 17 as a function of outdoor air temperature. Figure 17 (a) shows that the SPF3 values before the pump speed change were around 3, whereas Figure 17 (b) shows that the SPF3 values decreased to around 2.5 after increasing the pump speed. The reason for this significant decrease in the SPF values is the fact that the power required by the pump is proportional to the cube of the flow.

Compared to the DHW system, SPF3 values of the space heating system show a different trend. Firstly, as seen in Figures 18, the SPF3 values for the space heating system are generally higher than the DHW system. This is because the hot water produced by the heat pump in the space heating mode is at around 40 °C, whereas in the DHW mode the hot water is produced at around 60 °C. Secondly, the pump speed change also affected the efficiency of the space heating system. Figure 18 (a) and Figure 18 (b) show the SPF3 values of the space heating system before and after the pump speed change, respectively. As seen the SPF3 values of the space heating system decreased after increasing the pump speed.

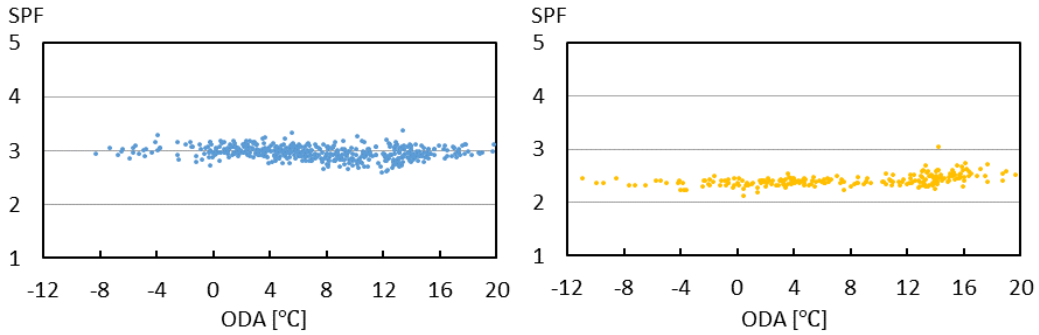

(a) (b)

Figure 17: Daily SPF3 values of the DHW system before (left) and after (right) the pump speed change.

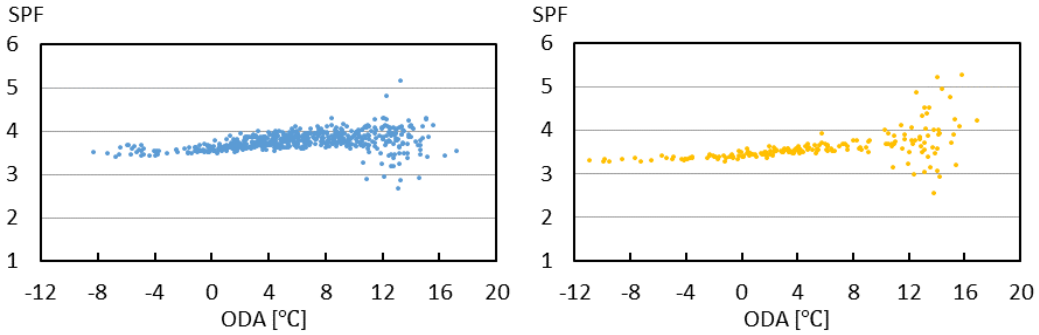

(a) (b)

Figure 18: Daily SPF3 values of space heating system before (left) and after (right) the pump speed change.

5 Case study 2

This chapter describes the second case study building, its ground cooling system, and the measurement setup. It also presents the results of the long-term measurements and performance evaluation of the ground cooling system.

5.1 System description

In recent years, it has become popular to use direct ground cooling (sometimes also called free ground cooling or passive ground cooling) using the ground heat exchangers. The direct ground cooling can be delivered to the conditioned space using either air or water system (or a combination of both). In some cases, the ground loads in a direct ground cooling system are balanced by extracting heat also to provide pre-heating or heating.

The concept of providing high-temperature cooling using a direct ground cooling system has been applied in the Entré Lindhagen building. The low-energy office building is the headquarter of Skanska, Sweden, and is located in Stockholm. The building is in operation since early 2014. The building comprises of nine office floors and has a net heated floor area of 65,265 m². The basement consists of a garage on three levels. The front elevation of the building is shown in Figure 19.

The building has been built with a vision to increase the use of renewable energy sources. The so-called Skanska's Deep Green Cooling (DGC) system has been installed at the building to provide cooling and air-conditioning. The DGC is a direct ground cooling system consisting of 144 boreholes, each 220-m deep, with double U-tube heat exchangers.

Figure 19: Picture of the Entré Lindhagen. (Source: group.skanska.com)

Compared to the conventional shallow geothermal cooling systems with chillers, the DGC system is more robust and more reliable (Gräslund, 2014). It operates without any mechanical

or thermal refrigeration system. It is easier to control and is more environmentally friendly. A schematic of the DGC system for the Entré Lindhagen building is shown in Figure 20. The figure shows the entire heating, cooling, ventilation, and domestic hot water (DHW) for this building. The main heating demand is covered by a district heating system. It provides space heating to the building through radiators. The DHW is also provided by the district heating system. Inlet water temperature for radiators is measured to be between 30–45 °C. The district heating is also used for air-conditioning the ventilation air in winter using the heating coils installed in the AHUs. The supply water to the air handling heating coils to heat the ventilation air is measured to be around 40 °C.

There are eight AHUs installed in this building. These AHUs provide 19–21 °C supply air throughout the whole year. Each unit consists of a pre-heating coil, an ambient- air cooling coil, a heat recovery system, an air heating coil, and an air cooling coil. The first coil is used to extract the heat stored in the ground in the summer by preheating the ventilation air. The second coil is used to provide free cooling to the building when the ambient air temperature is lower than the indoor temperature. This process also increases the temperature of the ventilation air provided to the building which is beneficial in winter. The third coil connected to the district heating system is to heat the ventilation air when required. The last coil is for air-conditioning of ventilation air in summer. It is connected to the DGC system through a heat exchanger. The AHUs are designed for low air velocities and low-pressure drops. The air velocity remains around 1.0 m/s through the coils and filters. Highly efficient heat recovery of over 80 % is used in each AHU.

In summer, the space cooling is provided by the direct ground cooling system through the chilled beams installed in the building. The direct ground cooling system is also used for air-conditioning the ventilation air in summer using the cooling coils installed in the AHUs. In winter, the ground cooling system pre-heats the incoming ventilation air. The preheating of ventilation air extracts the heat stored in the ground in summer and brings the ground temperature down. The entire cooling demands of the building, including the thermal comfort and process cooling, are met by the direct ground cooling and ambient-air cooling system. In the boreholes, the temperature level remains above freezing year-round, which makes it possible to use ordinary water in the ground loop. The water circulates in a closed-loop system with circulation pumps. Heat exchangers are used to exchanging the energy between the borehole loop and the circulation water loop in the building system. One important system component of the cooling system is the ambient-air cooling coil in the AHU. It provides free cooling to the chilled beams in the building when the outside temperature is below 20 °C and rejects the heat to incoming ventilation air to raise its temperature.

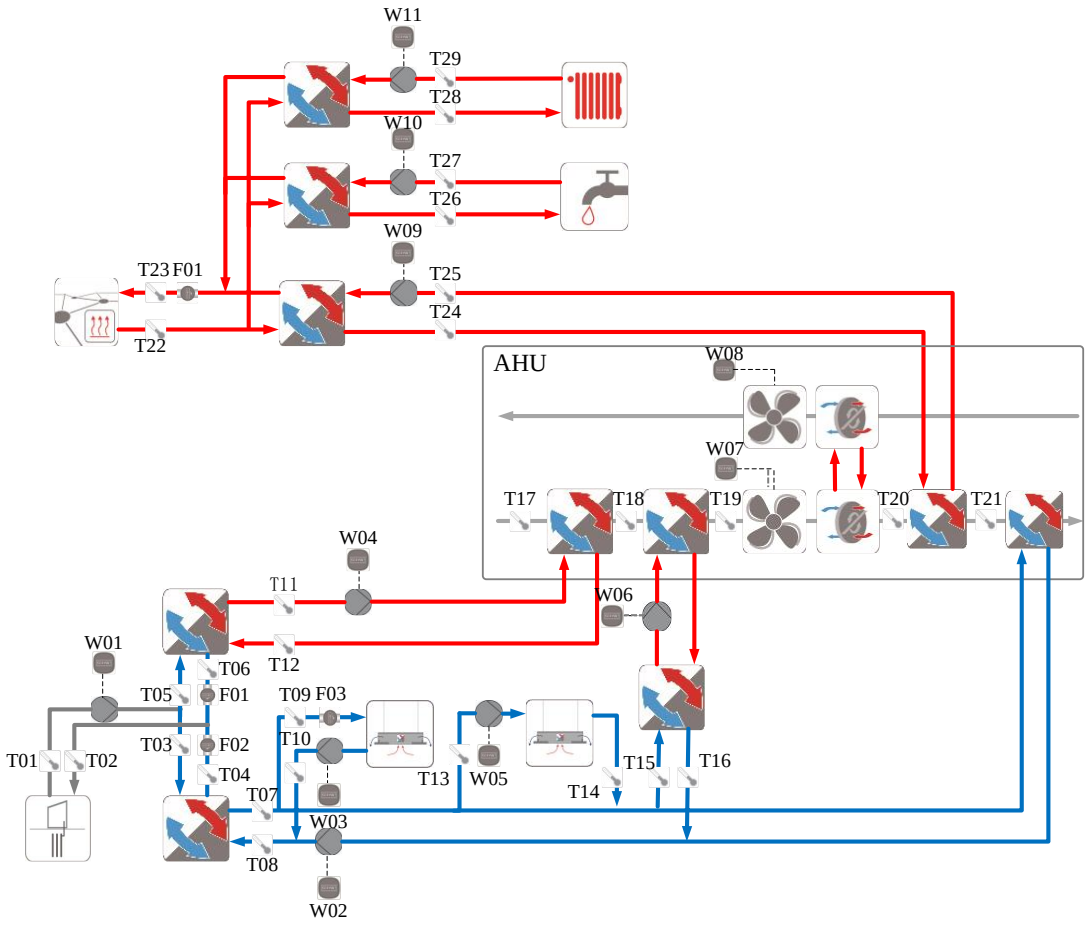

Figure 20: Schematic of the HVAC system of the Entré Lindhagen Building.[4]

5.2 Measurements

A robust and extensive monitoring and measurement system has been installed in the Entré Lindhagen building. The monitoring system collects high-frequency data with a 5 minutes resolution. For this study, five years of data from January 2014 to August 2018 has been used.

From the measured data, it is possible to calculate the delivered thermal energy and the consumed electrical energy of the whole system. In the hydronic system, temperature and flow sensors are present in all main heating and cooling circuits. Energy meters are used for recording gound heat extractions and injections. Besides, the electrical energy consumed by the circulation pumps is measured by electric meters with an accuracy of ±1 %.

[4] Pictograms in drawing used with permission from TU Braunschweig IGS.

The electric meters are used for measuring fan energy consumption in the AHUs. Temperature sensors are also present between all coils to measure the air temperature change.

In order to divide the electrical energy consumption of the AHU between heating, cooling, and ventilation, the actual pressure drops of the coils are used. It is possible to allocate the AHU electrical energy consumption based on the pressure drops (Spitler and Gehlin, 2019). The electrical energy consumption in the AHUs is calculated based on the pressure drop ratios as shown in Equation 14.

$$Energy_{coil,A} = \frac{\Delta P_{coil,A}}{\Delta P_{total}} * Energy_{total} \quad \text{[kWh]} \tag{14}$$

5.3 System boundaries

In order to evaluate the performance of the Entré Lindhagen deep green cooling system, appropriate system boundaries must be selected. As previously discussed, SEPEMO and Annex 52 boundary schemes have often been used in literature to evaluate the performance of GSHP systems. The SEPEMO boundary scheme is most suited for simple GSHP systems without many system components. On the contrary, Annex 52 boundary scheme has been proposed for performance evaluation of GSHP systems serving commercial, institutional, and multi-family buildings. It has more comprehensive system boundaries than the SEPEMO boundary scheme, which are well suited for larger and more complex systems. However, the deep green cooling system of Entré Lindhagen is quite unique as it does not have any heat pumps or chillers. This makes it difficult to apply either of the SEPEMO or Annex 52 boundary schemes for the performance evaluation of the Entré Lindhagen system. Nevertheless, some Annex 52 boundaries can still be applied to the cooling system of the building. This includes boundaries 0, 2, and 5+. Figure 21 shows the Annex 52 boundaries applied to the Entré Lindhagen system.

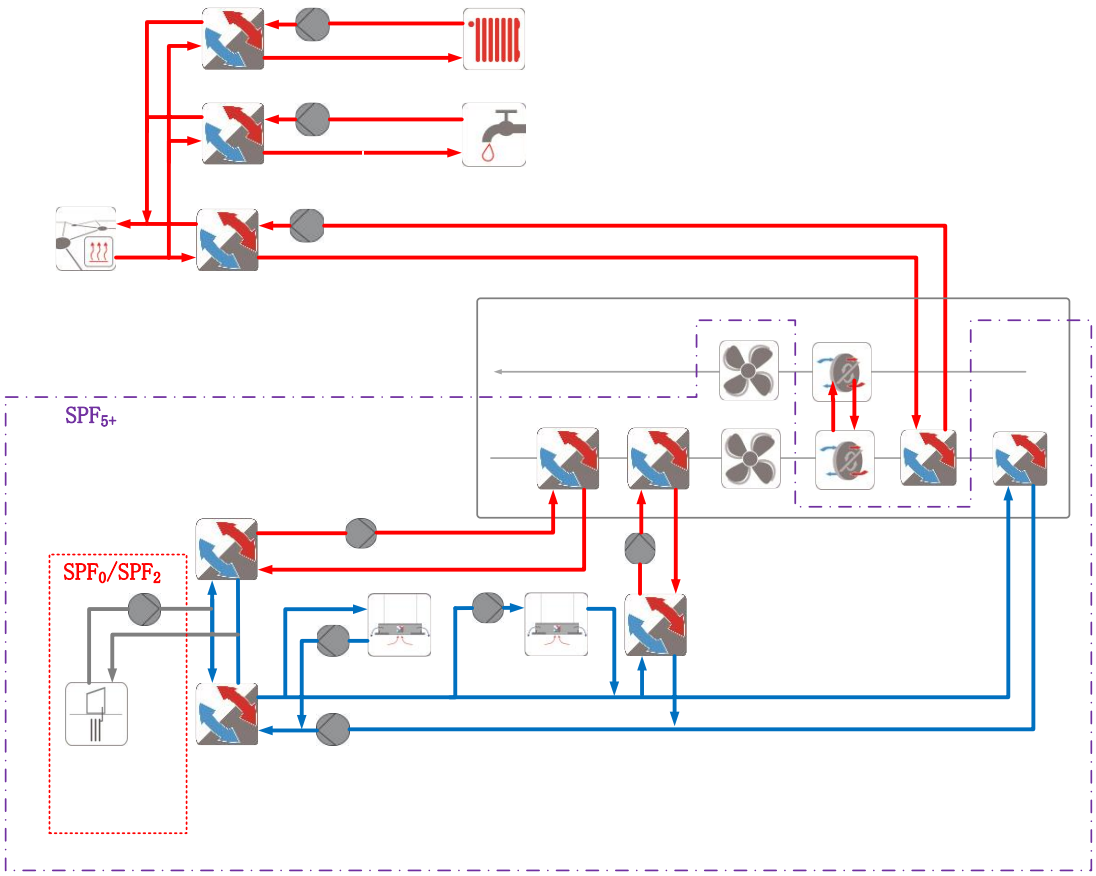

Figure 21: Annex 52 boundary scheme applied to the Entré Lindhage cooling system.[5]

SPF0 measures the seasonal performance of the borehole system. For SPF0, only the source-side pumps are considered. For the deep green cooling system, the SPF0 is also equal to the SPF2 and SPF2+, since it directly uses the ground source for cooling without compressors. The SPF2 boundary in Annex 52 also matches the SPF2 boundary in the SEPEMO boundary scheme. The SPF2 and SPF2+ provide a basis for comparing the performance of different systems, such as air-cooled chillers, water-cooled chillers, etc. It is not possible to apply SPF1, SPF3, and SPF4 boundaries to the DGC system. This is because the SPF1 calculates the compressor's performance but there are no chillers or heat pumps in this system. SPF3 and SPF4 evaluate the system performance before and after the buffer tanks, and there are no buffer tanks in the cooling system of Entré Lindhagen. However, the SPF5+ boundary, corresponding to the overall performance of the cooling system, can still be applied. For the Entré Lindhagen building, this boundary is applied to the entire cooling system, including the direct ground cooling and ambient-air cooling. SPF5+ is intended to present the overall performance of the system, including all circulation pumps, fans, and auxiliary components. Boundary 5+ extends to the distribution system, including all pumps and four coils in the

[5] Pictograms in drawing used with permission from TU Braunschweig IGS.

AHUs. There is one heating coil served by the district heating in the AHUs. However, the air heating coil is excluded from boundary 5+ as it is not a part of the cooling system. For the deep green cooling system, the SPFs are calculated as:

Table 5: Formulas for calculating SPFs.

$SPF_0 = SPF_2 = \frac{Q_{ghe}}{W_{p,s}}$
$SPF_{5+} = \frac{Q_{del}}{W_{p,s} + W_{p,d} + W_{Fan}}$

Indeed, it is possible to apply the SPF boundary 5+ differently. For example, to the heating and cooling system or the entire ground cooling and air conditioning system, including the AHU heating coil. However, any such application of the SPF boundary will mean the inclusion of district heating as auxiliary heating, which in turn will severely undermine the calculated performance of the cooling system.

5.4 Uncertainty analysis

The uncertainties in delivered thermal energy, consumed electrical energy, and calculated SPFs have been estimated to determine the reliability of results. The approach described by Spitler and Gehlin. (2019) has been used. The uncertainties have been calculated for monthly and yearly periods.

5.4.1 Thermal energy

The thermal energies in Entré Lindhagen building are measured by energy meters. The manufacturer provided fractional uncertainty for the energy meters is given by Equation 15.

$$e_q = \pm (0.5 + \frac{3}{\Delta T})\ \% \quad (15)$$

The absolute uncertainties are expressed as upper-case '*E*' and the fractional uncertainties are expressed as lower-case '*e*'. The fractional uncertainties of the thermal energy transfer rate can be converted to absolute uncertainties and integrated into absolute uncertainties using Equations 16 and 17.

$$E_q = e_q * q \quad (16)$$

$$E_Q = E_q * \Delta t \quad (17)$$

The monthly or annual thermal energy uncertainties can be calculated using Equations 18, and 19.

$$E_{Q,n} = \sum_{i=1}^{n} E_{Q,i} \tag{18}$$

$$e_{Q,n} = \frac{E_{Q,n}}{\sum_{i=1}^{n} Q_i} \tag{19}$$

5.4.2 Electrical energy Use

Electric meters have been used to monitor the electrical energy input of different components. The electrical energy meters used in the Entré Lindhagen have uncertainties of ±1 %. For each SPF boundary, the uncertainty of each component is considered. The uncertainty of the electrical energy consumed under boundary 0 and 5+ is determined using Equation 20.

$$E_W = \begin{cases} E_{p,s}, & \text{Boundary 0} \\ \sqrt{{E_{p,s}}^2 + {E_{p,\mathrm{d}}}^2 + {E_{Fan}}^2}, & \text{Boundary 5 +} \end{cases} \tag{20}$$

The monthly and yearly absolute uncertainties in energy consumption are calculated using Equation 21 and then converted into fractional uncertainties with Equation 22.

$$E_{W,n} = \sum_{i=1}^{n} E_{W,\mathrm{i}} \tag{21}$$

$$e_{W,n} = \frac{E_{W,n}}{\sum_{i=1}^{n} W_i} \tag{22}$$

5.4.3 Seasonal performance

Once the uncertainties in thermal energy delivered and electrical energy use have been calculated, the uncertainties in the seasonal performance factors can be determined. The uncertainties in thermal energy and electrical energy use can be added in quadrature using Equation 23 to determine the uncertainties in SPF values.

$$e_{SPF,n} = \sqrt{{e_{Q,n}}^2 + {e_{W,n}}^2} \tag{23}$$

5.5 Results

This section presents the results of measured data and analysis of the energy performance of the deep green cooling system in the Entré Lindhagen building for five years.

5.5.1 Ground heat exchange and load characteristics

To study the behaviour of the borehole system, the daily mean values for outdoor air temperature and the supply temperatures supplied from the borehole system are presented in Figure 22. The seasonal trends of borehole supply and outdoor air temperatures are similar. However, the borehole supply temperatures are much higher than the outdoor air temperature in winter and significantly lower than the outdoor air temperature in summer. An interesting aspect of the borehole supply temperatures is that the seasonal supply temperatures from the borehole system remain very steady over the years. As seen from the figure, the borehole supply temperatures in the summer are around 16 °C and in winter are around 9 °C. The seasonal-steady supply temperatures indicate that the annual ground heat injections and extractions are well balanced.

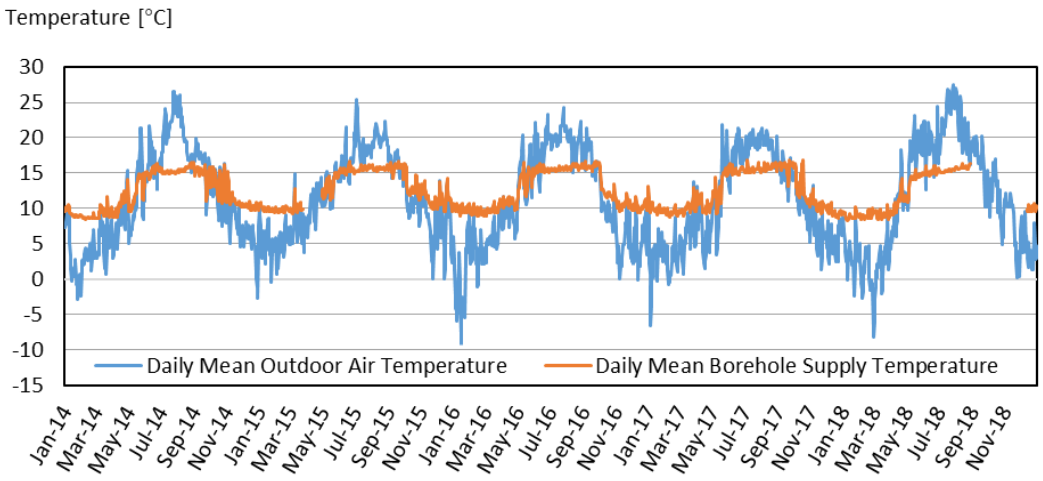

Figure 22: Daily mean borehole supply and outdoor air temperatures.

For the Entré Lindhagen system, the circulation pumps on the source-side are variable speed. The flow in the borehole system depends on the cooling demands in summer and on balancing-needs of the borehole system in winter. Figure 23 shows the mean daily borehole flows. The figure shows that the peak flow occurs when the heat injection to the ground or the extraction from the ground is maximum. The flows in spring and autumn are comparatively lower due to the lower ground heat injection or extraction during these periods.

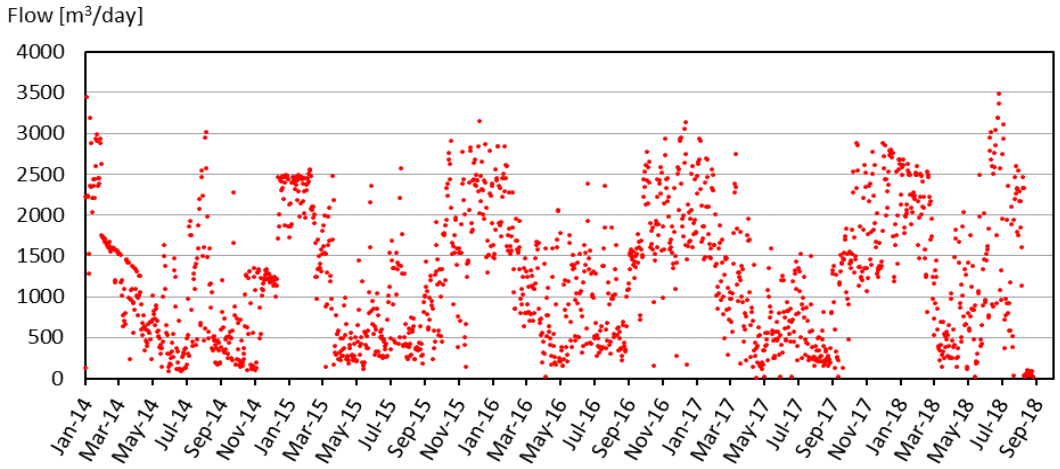

Figure 23: Daily mean borehole system flows.

The annual heat injection and extraction to and from the boreholes for five years are illustrated in Figure 24. Three-month data from September to November 2018 is not included due to data missing. The ground system started operating in 2014 and was commissioned during the first year of the building's operation. It can be seen that the highest heat injections to the ground occurred in 2018 as it had a very warm summer, as also seen from Figure 22. The values of ground heat extractions are nearly equal to the heat injections every year. Thus, the net ground heat injection and extraction over the five years have been quite balanced.

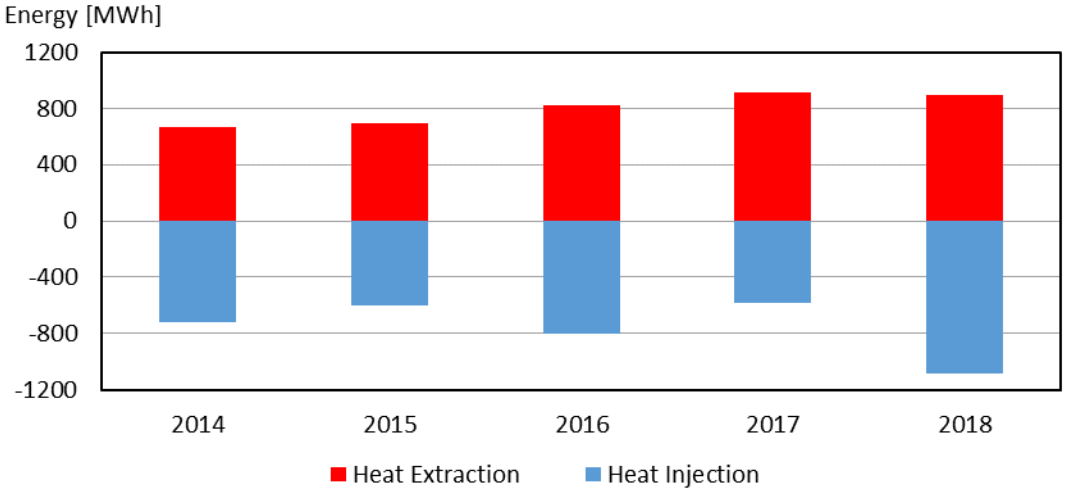

Figure 24: Ground heat extractions and injections.

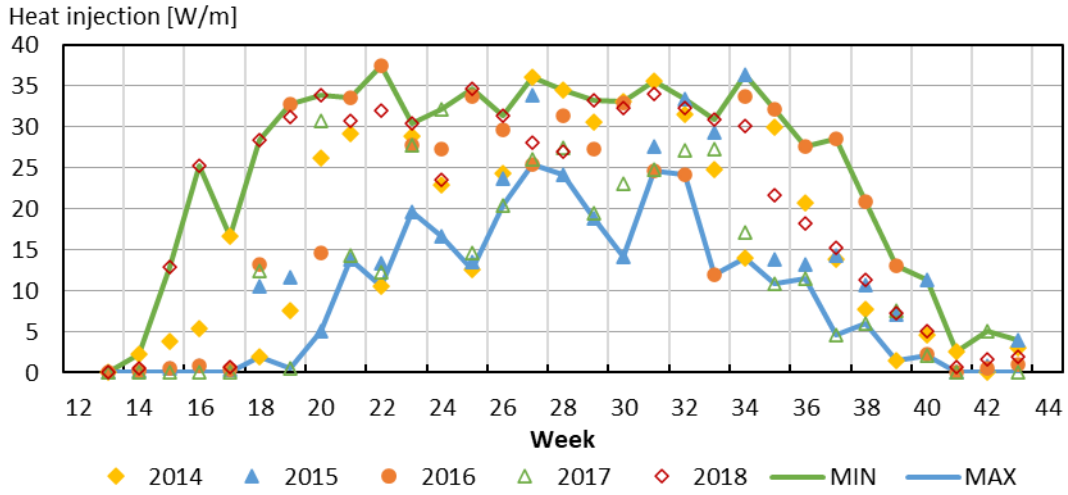

Figure 25: Specific heat injection rates

All boreholes in the Entré Lindhagen operate simultaneously. The weekly hourly maximum specific heat injection and extraction rates for the whole monitoring period of 2014-2018 are shown in Figure 25. The highest value of specific heat injection occurring in summer is around 35 W/m. The values are lower in spring and autumn. Besides, the ground heat injection is very low in winter but the ambient-air cooling coil is still used in winter to provide process cooling.

Figure 26 presents the weekly hourly maximum specific heat extraction rates for the whole monitoring period. The highest value occurs in winter and is below 25 W/m. The specific heat extraction rates are lower in spring and autumn and are zero in summer. Compared to the typical GSHP system, the specific heat extraction rates observed for the Entré Lindhagen building system are lower (Kyriakis et al., 2006). This is because the primary objective of ground heat extraction in the Entré Lindhagen system is to balance the net ground heat injection by preheating the ventilation air by 2–4 ℃.

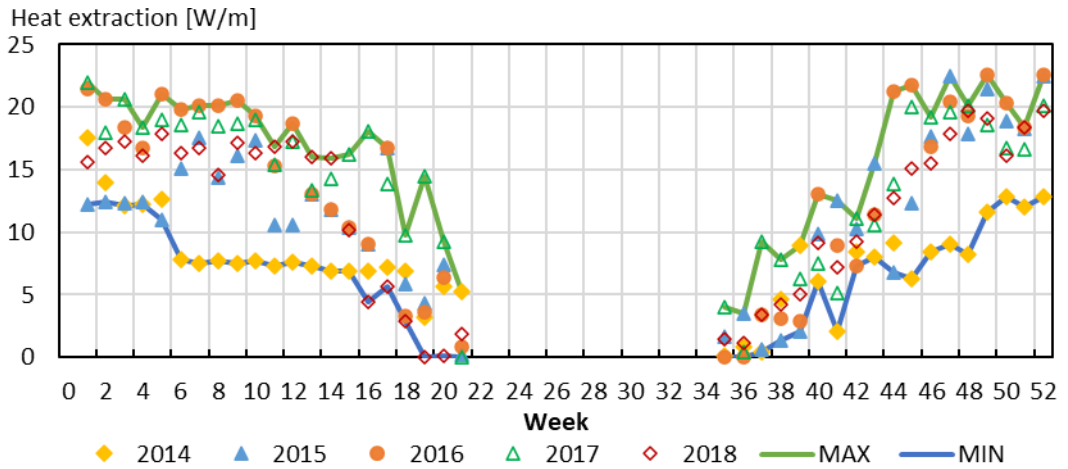

Figure 26: Specific heat extraction rates.

Figure 27 (a) illustrates the average delivered energy from the borehole system in heat injection and extraction modes as a function of the outdoor air temperature. The figure also presents the average delivered energies from the ambient-air cooling coil (Figure 27 b), and district heating (Figure 27 c) as well as the whole building heating and cooling loads (Figure 27 d). All values shown in the figure are calculated based on hourly average values. The entire cooling demand of the building including the process cooling throughout the whole year is covered by the direct ground cooling system and the ambient-air cooling coil. The peak loads in heat injection mode are almost two-fold higher than the peak load in heat extraction mode. However, it shall be noted again that the heat extraction system works only for pre-heating the ventilation air when the outdoor air temperature is lower than 15 °C, to keep the ground thermally balanced over the year. The ambient-air cooling coil contributes to both cooling and pre-heating systems. It recycles the waste heat from the return side of the chilled beams and uses it to pre-heat the ventilation air. The peak load covered by the ambient-air cooling coil is around 130 kWh/h, as seen in Figure 27 (b). It only operates when the outside air temperature is lower than 20 °C. The district heating loads are seasonal and are negatively correlated with outdoor air temperature as seen in Figure 27 (c). The district heating is responsible for all space heating delivered by the radiators, for all DHW loads, as well as for heating the ventilation air to the desired supply temperature level after the heat recovery. The peak district heating load is around 900 kWh/h. As shown in Figure 27 (d), the peak heating loads of the building are around 2800 kWh/h. The heat recovery and pre-heating of ventilation air in the AHU make up for the difference between the building heating demand and the heat supplied by the district heating. The peak cooling load is approximately 700 kWh/h and is quite low compared to the peak heating load.

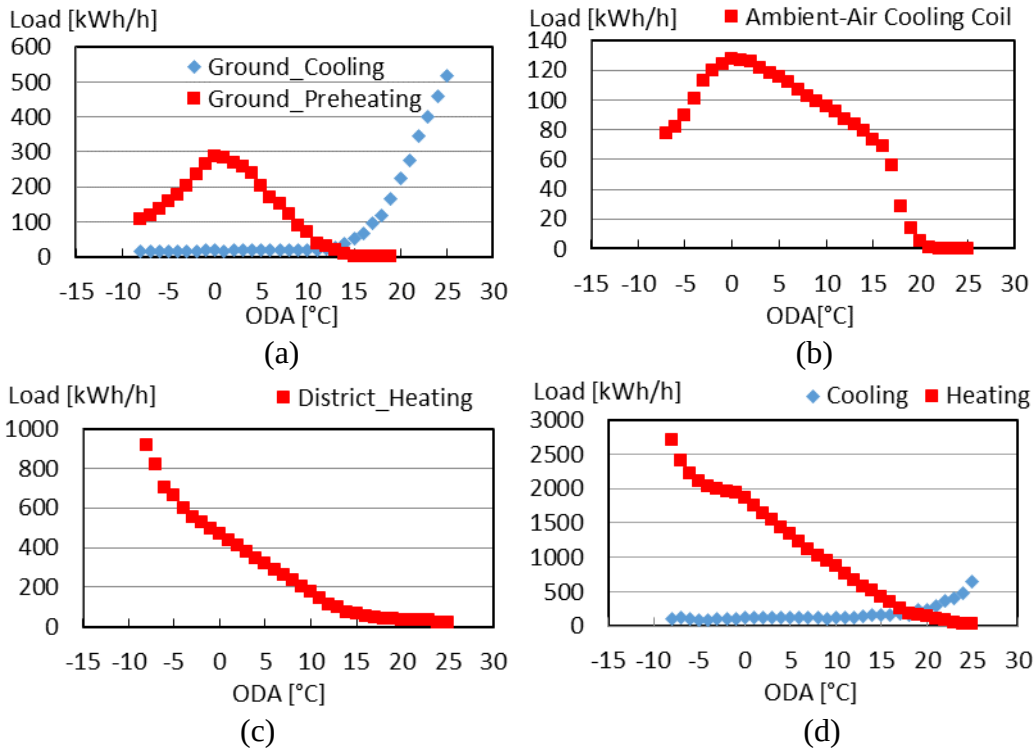

Figure 27: Measured energy signature of (a) ground-source, (b) ambient-air cooling coil, (c) district heating, (d) the whole building.

5.5.2 Energy performance

Figure 28 shows the yearly delivered heating and cooling energies to the Entré Lindhagen building and the electrical energy consumption of all fans and pumps. It can be seen from the figure that ventilation heat recovery accounts for over 50 % of the total delivered heating energy to the building. The district heating provides almost 25 % of the total delivered heating energy. The borehole heat exchangers and the ambient-air cooling coil both provide over 500 MWh of heating energy every year. The total delivered heating energy during the first year of operation was relatively higher due to the lower internal heat gains because of lower occupancy and due to the ongoing adjustments of the system. The cooling energy is provided by the ground cooling system and by the ambient-air cooling coil in the air handling. The cooling energy output of the ambient-air cooling coil and the ground cooling is almost similar. Overall, the building energy consumption for heating and cooling is dominated by heating energy, which is almost five times greater than the delivered cooling energy.

The annual electrical energy used by different components of the HAVC system is also shown in the following figure. As the system operates without any compressors, the electrical energy consumption only comprises of the energy consumed by the pumps and the fans. The electrical energy consumed by the AHU fans accounts for about 75 % of the total electrical energy consumption. The electrical energy consumed by the circulation pumps is approximately 25 % of the total electrical energy consumption.

The electrical energy used by the fans is divided into energy consumed for providing ventilation, and for overcoming the pressure drop of various pre-heating and cooling coils in the AHU. The electrical energy consumed for providing the ventilation accounts for approximately half of the total electrical energy consumption of the fans. The electrical energy consumed for overcoming the pressure drops of heat recovery coil is 32 %, for district heating coil is 2 %, for the main cooling coil is 6 %, for pre-heating coil is 1 %, and for ambient-air cooling coil is 9 % of the total electrical energy consumption.

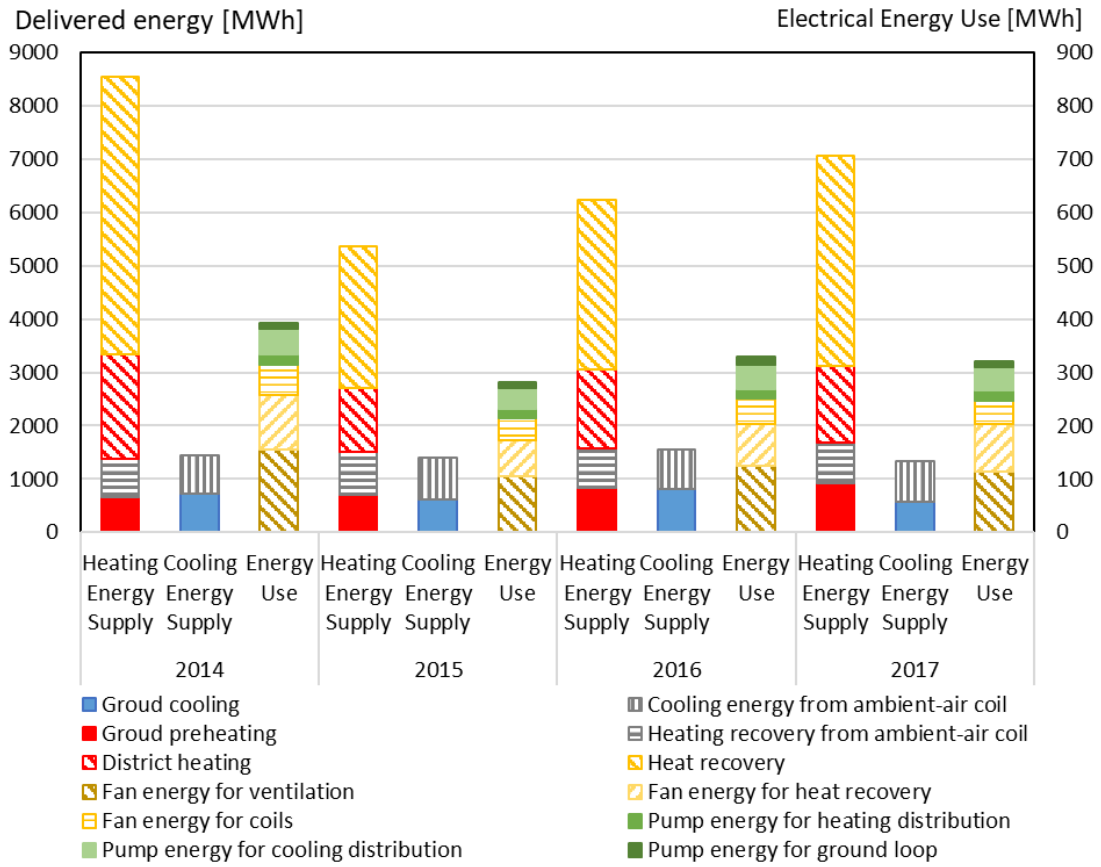

Figure 28: Annual delivered heating and cooling, and electrical energy use.

In order to further elaborate the heating and cooling demand, the monthly delivered heating and cooling energies for 2016 are presented in Figure 29. The ambient-air cooling coil provides both cooling and pre-heating at the same time. It cools the return water from chilled beams and uses the heat from this return water to pre-heat the ventilation air. The ambient-air cooling coil is most efficient in spring and autumn when there is moderate cooling demand and the outdoor air temperature is low enough for providing free cooling. The cooling supplied by the ambient-air cooling coil decreases in summer with increasing outdoor temperatures. The ground cooling serves the building mainly in summer providing both comfort and process cooling. The energy output of ground cooling is lower in periods when the ambient-air cooling coil can be used. For periods when ambient-air cooling coils cannot be used, the output of the ground cooling system is significantly higher.

For the heating energy, heat recovery provides the largest part throughout the year followed by the district heating system. The ground system is used in winter for pre-heating the ventilation air to balance the ground heat injection in months from January to May and October to December. It provides a considerable amount of heating energies in the form of ventilation preheating.

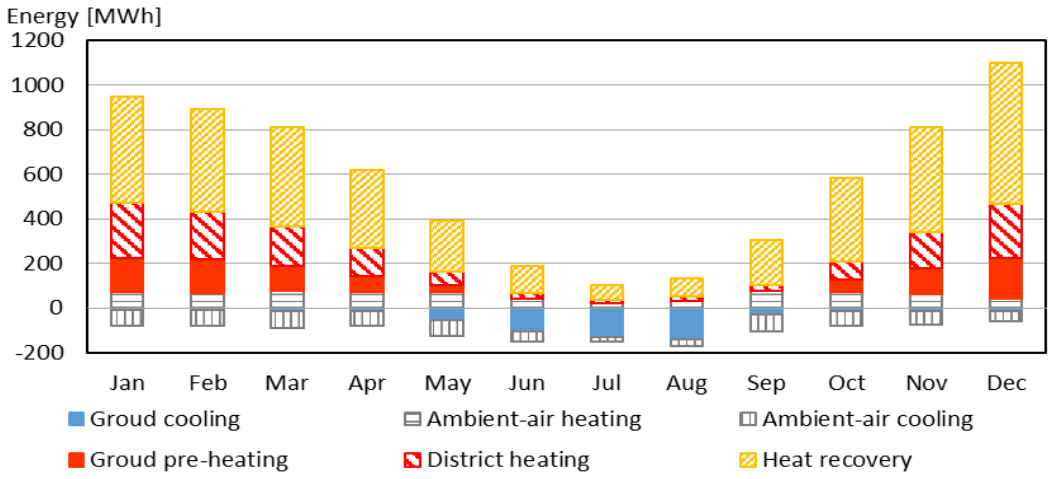

Figure 29: Monthly delivered heating and cooling energies in 2016.

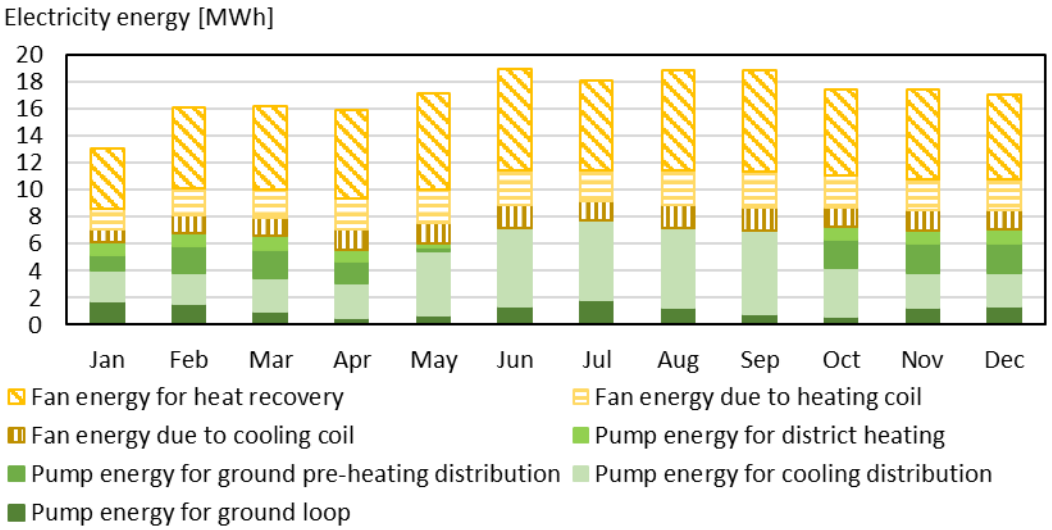

Figure 30: Monthly electrical energy consumption of heating and cooling system components in 2016, excluding ventilation fan energy.

The monthly electrical energy used by the HAVC system components for 2016 is shown in Figure 30. The pumping energies for ground cooling and ambient-air cooling are both considered in cooling distribution energies. As expected, the electrical energy use of pumps for the distribution of heating and cooling is seasonal. The pumps providing extracted heat from the ground for pre-heating the ventilation air only work in winter. The distribution pumps providing cooling to ventilation air have higher electrical energy consumption in summer than in winter when they only provide process cooling. The lowest energy use of borehole-side pumps is seen in spring and autumn as the ground provides less thermal energy in these seasons.

To divide the electrical energy used by the fans between different components, the electrical energy consumption of the fans is divided based on the pressure drops induced by these components. Figure 30 provides details of fan energy distribution between different components. The heat recovery coil is responsible for the largest portion of the fan energy due to its high-pressure drop.

5.5.3 Seasonal performance factors

In this section, the seasonal performance factors are presented for the Entré Lindhagen DGC system using Annex 52 boundaries. The annual values of $SPF2_{cooling}$ and $SPF5+_{cooling}$ are presented in Figure 31. The Y-axis has a logarithmic scale of base 2. The annual $SPF2_{cooling}$ values vary from 119 ± 2.4 to 152 ± 3.1. For typical GSHP systems, this factor is from 4.0 to 6.8 (Spitler & Gehlin, 2019). This means the direct ground cooling system is several folds more energy-efficient than typical GSHP systems. The $SPF5+_{cooling}$ takes into account the cooling provided by the ground system and the ambient-air cooling coil. The $SPF5+_{cooling}$ presents the overall performance of the cooling system including both the ground cooling system and ambient-air cooling system. The $SPF5+_{cooling}$ values range between 14 ± 0.9 and 17 ± 0.3. The decrease in SPF values between boundaries 2 and 5+ indicates the impact of the energy consumption of the fans and pumps on the performance of the system. Nevertheless, compared with the traditional heat pump systems, the $SPF5+_{cooling}$ values are also several folds higher indicating excellent energy performance of the DGC system.

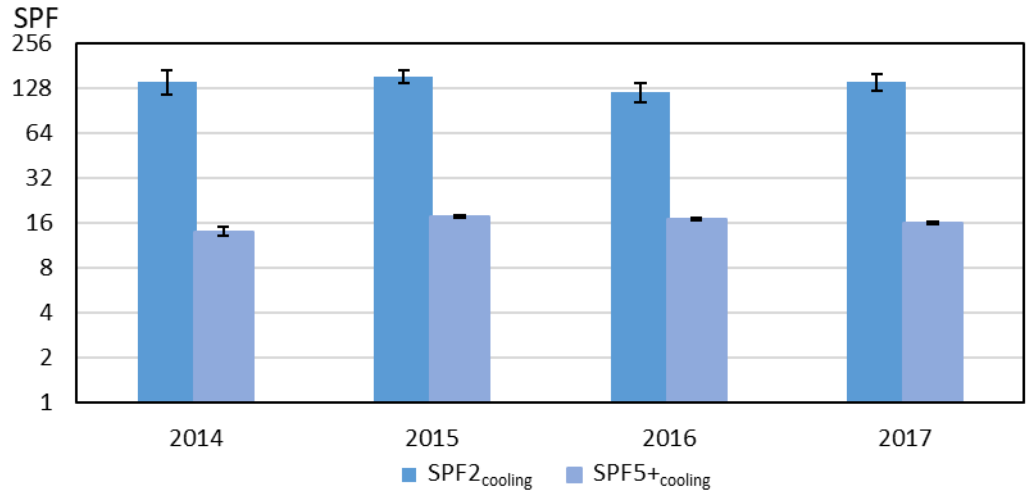

Figure 31: Annual SPFs in cooling mode.

Additionally, the annual SPFs of the DGC system in the pre-heating mode are shown in Figure 32 for Annex 52 boundary. The Y-axis again has a logarithmic scale of base 2. The $SPF2_{heating}$ values are between 103 ± 17 and 162 ± 25. The typical $SPF2_{heating}$ values for GSHP systems are generally between 2.2 and 5.9 (Spitler & Gehlin, 2019). The $SPF5+_{heating}$ values for the DGC system are between 29 ± 6.2 and 37 ± 4.7. These values account for heating provided by the ground system and the ambient-air cooling coil.

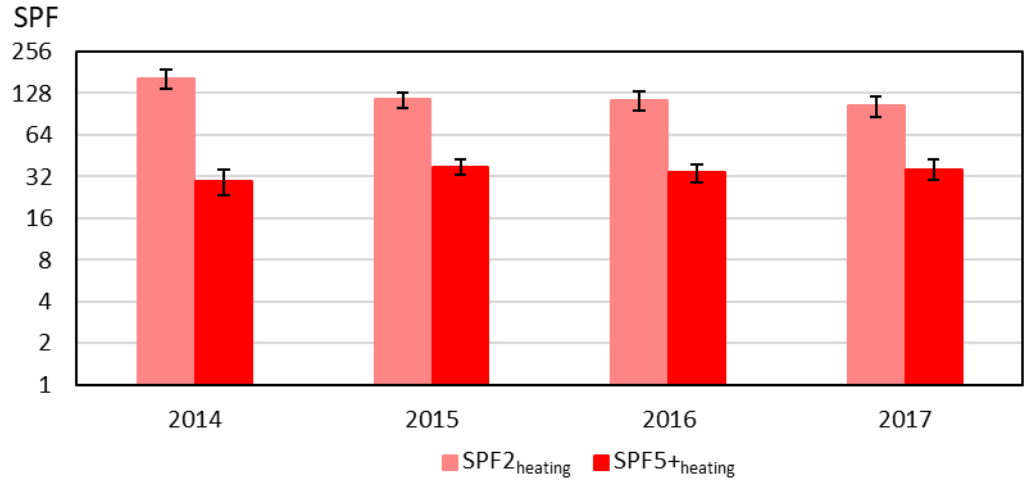

Figure 32: Annual SPFs in the pre-heating mode.

To study the detailed system performance, monthly cooling SPFs for 2016 are presented in Figure 33. The Y-axis has a logarithmic scale of base 2. The $SPF2_{cooling}$ and $SPF5+_{cooling}$ values vary in a range between 84 ± 2.1 and 139 ± 3 and between 10 ± 0.1 and 18 ± 0.3, respectively. The seasonal fluctuation is mainly due to two factors, ground supply temperature, and distribution system efficiency. These two factors, however, influence the performance differently. As shown in Figure 21, the borehole supply temperatures are lower in winter, and hence they provide a better cooling performance in winter. On the other hand, the cooling load is lower in winter, and hence the borehole side circulation pumps operate at lower speeds and reduced efficiencies. Combining these two factors results in peak $SPF2_{cooling}$ values occurring in spring and autumn. The monthly $SPF5+_{cooling}$ values are significantly lower than the $SPF2_{cooling}$ values due to the energy consumption of the distribution system. In summer, the circulation pumps work at design speeds and at high efficiencies, which results in peak $SPF5+_{cooling}$ occurring in summer.

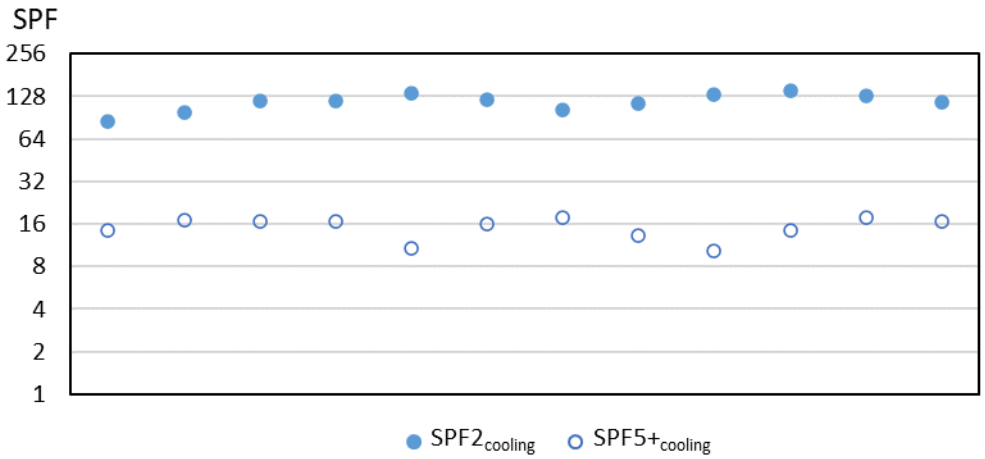

Figure 33: Monthly cooling SPFs for 2016.

Figure 34 presents $SPF2_{heating}$ and $SPF5+_{heating}$ for 2016. The Y-axis has a logarithmic scale of base 2. The system boundaries only cover the pre-heating of ventilation air through the ground system and the ambient-air cooling coil. The SPF values are not shown for summer as there is no pre-heating of ventilation air in summer months. The monthly $SPF2_{heating}$ and $SPF5+_{heating}$ values vary between 106 ± 15 and 189 ± 33 and between 30 ± 5.3 and 45 ± 6.7, respectively. As with annual SPF values, the energy consumption of the distribution system brings the performance down. It can be noticed that the $SPF2_{heating}$ values are higher in spring and autumn than in winter. This can be explained by the higher ground temperature in spring and autumn than in winter. On the other hand, the $SPF5+_{heating}$ values show an opposite trend and they are lower in spring and autumn than in winter. It is because the ventilation air has lower pre-heating requirements in spring and autumn, and consequently the pumps operate at part-load conditions at lower efficiencies.

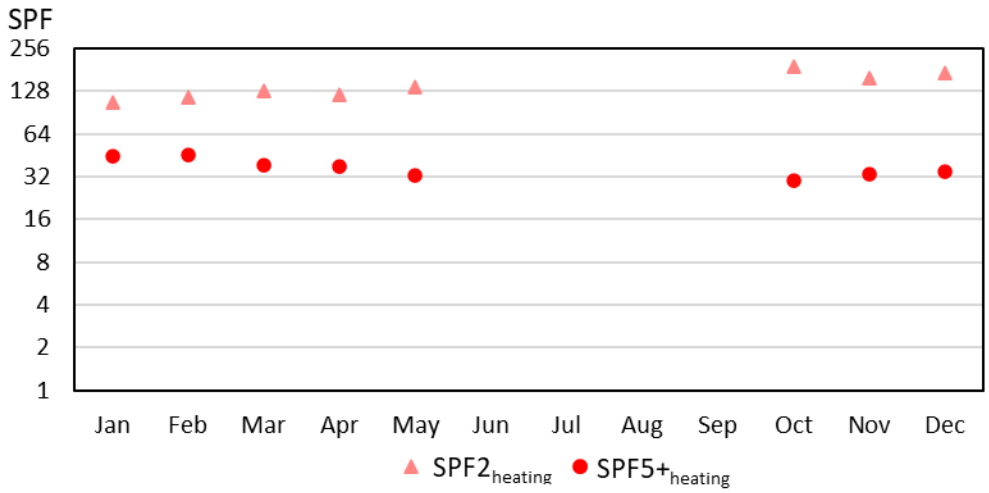

Figure 34: Monthly pre-heating mode SPFs for 2016.

Figure 35 (a) and (b) show the monthly values of $SPF5+_{cooling}$ and $SPF5+_{heating}$ for the 2014 to 2018 period. Four months of data from January to April 2014 is not included due to the ongoing adjustments of the system and lower internal heat gains and occupancy. For the cooling performance, the seasonal trends in different years are similar and most of the $SPF5+_{cooling}$ values vary around 15. The highest $SPF5+_{cooling}$ occurs in July 2014 and is 23.4. For heating, the $SPF5+_{heating}$ values vary in a larger range, and the trends of different years are similar. The highest $SPF5+_{heating}$ value occurs in January 2016 and is 47.8. In summary, the actual SPF values fluctuate in different years but the overall variation trends remain similar.

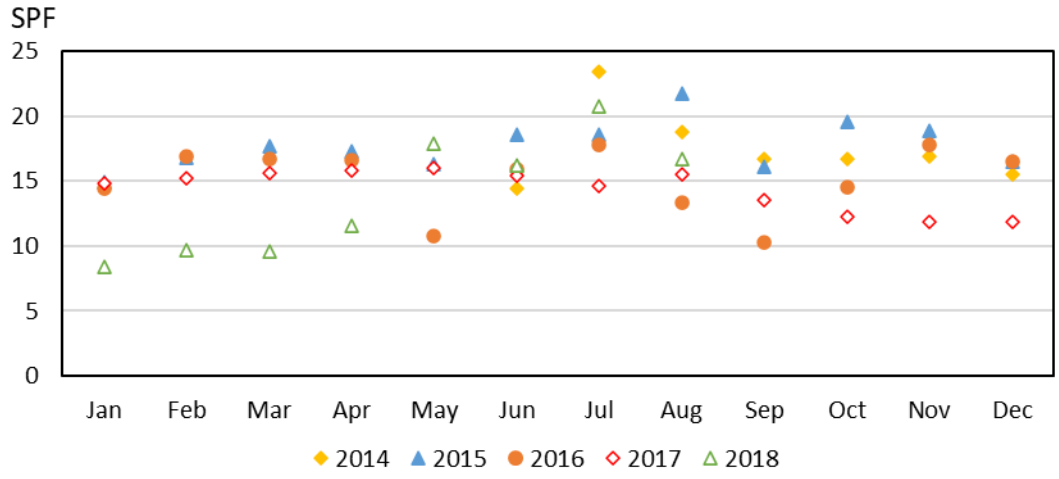

(a)

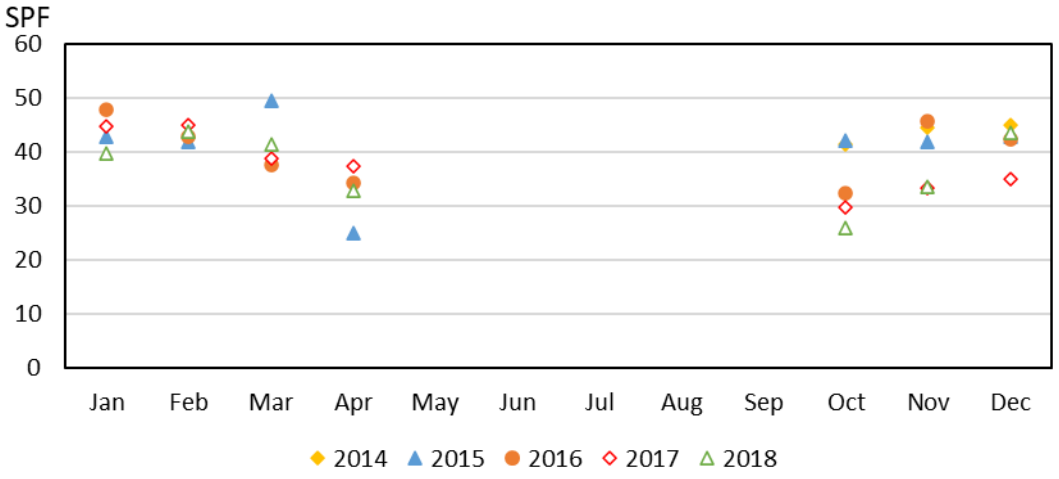

(b)

Figure 35: Monthly (a) $SPF5^{+}_{cooling}$ and (b) $SPF5^{+}_{heating}$.

6 Discussion and Conclusions

In this study, the performance of two ground-source systems has been analyzed based on different system boundary schemes. SEPEMO and Annex 52 boundary schemes have been used to analyze the system performance of the first system. Compared to the SEPEMO scheme, Annex 52 method has been shown to provide more detailed results. Although all SEPEMO boundaries match one of the Annex 52 boundaries, it is better suited for smaller systems with fewer components.

When analyzing the performance of the second system, it has been noted that both the SEPEMO and Annex 52 boundary schemes are not wholly applicable. Although both these two schemes are designed for the ground-source system, the real projects can be more complex and the application of the standard proposed schemes may not be viable. When evaluating a multi-source or a direct ground cooling system, customized system boundaries may be needed.

Additionally, for any boundary scheme, the monitoring results from sensors play a vital role in calculating the SPFs. The long-term performance measurement of ground heating and cooling systems highly depends on the sensor installation and monitoring settings, such as frequency, parameters, instrument quality, etc. The smaller the monitoring interval, the more detailed the investigation and optimization can be (Bockelmann and Fisch, 2019). In the first system, all sensors provided data with a 2-minutes interval. The high-resolution data made it possible to present the results for different periods, including hourly, daily, monthly, and annually. The annual SPF results have been calculated to show the yearly system performance under different boundary schemes. However, to investigate the detailed system performance monthly SPFs have also been calculated. Moreover, some detailed analysis has also been performed using hourly and daily time steps.

Although high-precision instruments were installed in both systems, yet the uncertainty analysis of the results is still vitally important. For both case studies, uncertainty analysis has been carried out based on the uncertainty information provided by the measurement equipment manufacturers. The measurement uncertainties of the sensors have been used to determine the uncertainties in thermal energies, electrical energies, and monthly and yearly SPFs. For the first system, the highest uncertainty is attributed to the calculated heat pump delivered energy. It has an uncertainty of approximately 6.6 %. Electrical energy consumption has a maximum uncertainty of 4.6 %. The larget uncertainty in the annual SPFs is 8 % for Annex 52 boundary 3+, for 2014. For the second system, the highest uncertainty is attributed to the electrical energy consumption of pumps and fans. The uncertainty in the electrical energy consumption of these components is 6.4 %. The uncertainty in the delivered thermal energy from the ground source is 1.3 %. Finally, the largest uncertainty in annual SPFs is for $SPF5+_{cooling}$ and is 6.6 %.

Another interesting aspect worth discussing is the borehole heat exchanger characteristics. In the first case study, the GSHP system is coupled with a single borehole heat exchanger, which only covers the heating demand of the clubhouse. The measured specific heat extraction rates were rarely above 15 W/m. Comparing the measured specific heat extraction rates with the common range of specific heat extraction rates of 50–70 W/m (VDI 4640, 2001) suggests that this borehole heat exchanger has been rather oversized. The same can also be noticed from

the relatively stable and high borehole supply temperature over the three years of the monitoring period, shown in Figure 5. In the second system, the maximum specific heat injection rates occur in summer and are around 35 W/m. The maximum specific heat extraction rates occur in winter and are below 25 W/m. Considering it is a direct ground cooling system, the primary objective of the heat extractions in the Entré Lindhagen building is to balance the ground heat injections.

One significant feature of the Entré Lindhagen system is the ambient-air cooling coil in the AHU. The performance of the ambient-air cooling coil has been analyzed based on five years of monitoring data. In fact, it contributes to both cooling and pre-heating sides. As Figure 36 (a) shows, the ambient-air cooling coil works for approximately 3000 hours a year. The supply fluid temperature to the coil is between 19–22 ℃. Thus, it pre-heats the ventilation air by 1–3 ℃ when the outdoor air temperature is lower than 22 ℃, as shown in Figure 36 (b). By recycling the waste heat from the return side of the chilled beams, the ambient-air cooling coil not only covers half of the building's cooling demand but also contributes to the pre-heating of the ventilation air.

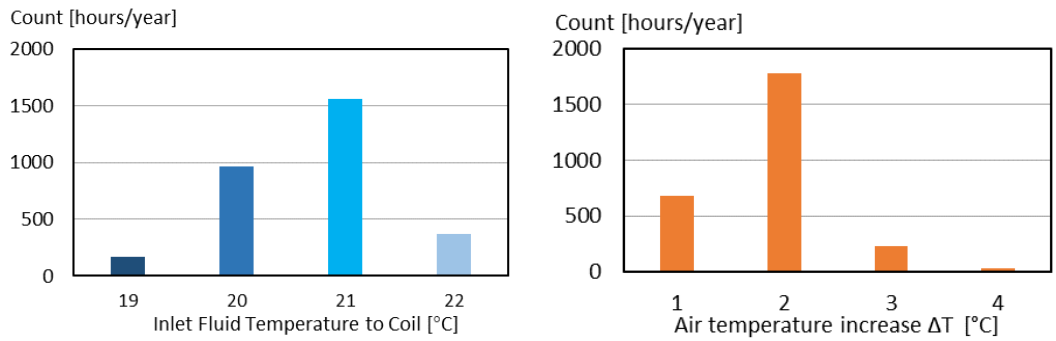

Figure 36: Ambient-air cooling coil's (a) entering fluid temperature and (b) air temperature increase.

Entré Lindhagen building uses a direct ground cooling system. The supply temperatures from the ground system are around 16 ℃ in the cooling mode. The direct ground cooling system not only saves energy but is also simple and effective. The direct ground source system at Entré Lindhagen has been well designed. It is not only used for providing direct ground cooling but also pre-heats the ventilation air to balance the ground loads while simultaneously reducing the heating energy consumption.

Two ground-source systems have been evaluated using measured data over a period of three and five years, respectively. The efficiency of the two systems has been analyzed in terms of Seasonal Performance Factors. Summary of the key findings of this study in the following.

- The first system is a small-sized GSHP system. For this system, the annual SPF values for SEPEMO boundary scheme range between 3.6 ± 0.22 and 3.9 ± 0.24 for boundary 1 to between 2.2 ± 0.16 and 2.3 ± 0.17 for boundary 4 over the three years measurement period. The difference between SPF1 and SPF4 is due to auxiliary components in the system.

- For the first system, the annual SPF values for Annex 52 boundary scheme range between 33.4 ± 2.0 and 34.9 ± 2.1 for boundary 0 to between 2.2 ± 0.16 and 2.3 ± 0.17 for boundary 3+ over the three years measurement period. The difference in values of SPF0 and SPF3+ is due to the compressor and auxiliary components in the system.

- For the first system, SPF values decrease dramatically between SEPEMO boundaries 1 and 4. For example, in 2014, the SPF annual values dropped from 3.9 ± 0.24 to 2.3 ± 0.17 between boundaries 1 and 4. The auxiliary components in the system, especially the electric heaters, significantly decrease the system performance.

- The second system is a direct ground cooling system installed in an office building. For this system, the annual SPF values for Annex 52 boundary scheme in cooling mode range between 119 ± 2.4 and 152 ± 3.0 for boundary 2 to 14 ± 0.9 and 17 ± 0.3 for boundary 5+ over the five years measured period. The difference in values of $SPF2_{cooling}$ and $SPF5+_{cooling}$ is due to the system consumption of the distribution system.

- The ambient-air cooling coil is a highlight of the second system. Combined with the direct ground cooling system, it demonstrates huge advantages for both cooling and preheating. The ambient-air cooling coil not only covers almost half of the building's cooling demand but also contributes to preheating the ventilation air.

- When using an air-distribution system as in the second system, a possible way of dividing the fan energy consumption between heating, cooling, and ventilation is by using pressure drop ratios of the components in the AHU.

- The SPF0 values for Annex 52 boundary scheme range between 33.8 ± 2.0 to 34.9 ± 2.1 for the first system over the three years measured period. The SPF0 values for the second system range between 119 ± 2.4 to 152 ± 3.1 over the five years measured period. The first system is a ground source heat pump system, whereas the second system is a direct ground cooling system.

- Auxiliary components operating at non-optimal conditions may cause a significant negative impact on the whole system performance. The circulation pumps and auxiliary heater operating at non-optimal conditions in the first system are shown to impact the performance considerably.

- Based on the evaluation of the first system, it can be claimed that the Annex 52 boundary scheme provides a more comprehensive performance evaluation than the SEPEMO boundary scheme. However, based on the evaluation of the second system, it is also demonstrated that even Annex 52 boundary scheme is difficult to apply on multi-source and direct ground systems.

References

Bockelmann, F., Norbert Fisch, M. (2019) 'It Works—Long-Term Performance Measurement and Optimization of Six Ground Source Heat Pump Systems in Germany', *Energies* 12(24),4691

Busato, F., Lazzarin, R.M., Noro, M. (2013) 'Two Years of Recorded Data for a Multisource Heat Pump System: A Performance Analysis', *Applied Thermal Engineering* 57(1-2), pp. 39-47.

Carlini, M. and Castellucci, S. (2011) 'Modelling the vertical heat exchanger in the thermal basin', in *Proceedings of the International Conference on Computational Science and Applications* (ICCSA '11), vol. 6785 of Lecture Notes in Computer Science, part 4, pp. 277–286, Springer, Santander, Spain.

de Klijn-Chevalerias, M. and Javed, S. (2017) 'The Dutch approach for assessing and reducing environmental impacts of building materials', *Building and Environment* 111, pp. 147-159

Duque, M.R., Pascoal, J. (2014) 'Heating and cooling a building using water from boreholes', *International Conference on Renewable Energies and Power Quality* 1(12), 492, pp. 802-805 [Online] Available at: https://www.researchgate.net (Accessed June 2020)

European Parliament. (2010) 'Directive 2010/31/EU of the European Parliament and of the Council of 19 May 2010 on the energy performance of buildings (recast)', *Journal of the European Union*, 153, 18.6.2010, p. 13–35 [Online] Available at: http://data.europa.eu/eli/dir/2010/31/oj (Accessed April 2020)

Gehlin, S., Andersson, O. (2019) 'Geothermal Energy Use, Country Update for Sweden', *European Geothermal Congress 2019* Den Haag, The Netherlands, 11-14 June 2019

Gehlin, S., Spitler, J.D. (2020) 'Half-term Results from IEA HPT Annex 52 - Long-term Performance Monitoring of Large GSHP Systems', *13th IEA Heat Pump Conference* May 11-14, 2020 Jeju, Korea

Geng, Y.; Ji, W.; Wang, Z.; Lin, B.; Zhu, Y. (2019) 'A review of operating performance in green buildings: Energy use, indoor environmental quality and occupant satisfaction'. *Energy and Buildings* 183, pp. 500-514

Gleeson, C.P., Lowe, R. (2013) 'Meta-analysis of European heat pump field trial efficiencies', *Energy and Buildings* 66, pp. 637-647

Gräslund, J (2014) 'nZEB headquarters of Skanska', *The REHVA Europen HVAC Journal* 51(2) March, pp. 44-47

Hassan, N and Javed, S (2019), 'Comparative life-cycle assessment of constant air volume, variable air volume and active climate beam systems for a Swedish office building', in *Proceedings of the 40th AIVC Conference: From energy crisis to sustainable indoor*

climate – 40 years of AIVC., D1_S4C-13, Air Infiltration and Ventilation Centre - AIVC, pp. 627-636, 40th AIVC - 8th TightVent - 6th venticool Conference, Ghent, Belgium, 2019/10/15.

Hwang, Y., Lee, J.-K., Jeong, Y.-M., Koo, K.-M., Lee, D.-H., Kim, I.-K., Jin, S.-W., Kim, S.H. (2009) 'Cooling performance of a vertical ground-coupled heat pump system installed in a school building', *Renewable Energy* 34, 578–582.

Javed, S (2012) 'Thermal modelling and evaluation of borehole heat transfer'.

Javed, S, Ørnes, IR, Myrup, M & Dokka, TH (2019) 'Design optimization of the borehole system for a plus-Energy kindergarten in Oslo, Norway', *Architectural Engineering and Design Management*, vol. 15, no. 3, pp. 181-195. https://doi.org/10.1080/17452007.2018.1555088

Kurkinen, E.-L., Filipsson, P., Elfborg, S., Ruud, S. (2014) *Skillnad Mellan Beräknad och Verklig Energianvändning—Energistyrning Under Byggprocessen—Slutrapport December 2014. SP Sveriges Tekniska Forskningsinstitut: Borås, Sweden.* [Online] Available at: http://www.diva-portal.org/smash/get/diva2:962872/FULLTEXT01.pdf (Accessed May 2020)

Lazzarin, R., Noro, M. (2013) 'Lessons Learned from Long Term Monitoring of a Multisource Heat Pump System', *Energy and Buildings* 174: 335–46

Li, C., Hong, T., Yan, D. (2014) 'An insight into actual energy use and its drivers in high-performance buildings', *Applied Energy* 131, pp. 394-410

Liu, X., Malhotra, M., Im, P. (2017) 'Performance Analysis of Ground Source Heat Pump Demonstration Projects in the United States', *12th the IEA Heat Pump Conference 2017* [Online] Availiable at: http://hpc2017.org/wp-content/uploads/2017/05/P.2.7.16-Performance-Analysis-of-Ground-Source-Heat-Pump-Demonstration-Projects-in-the-United-States.pdf (Accessed April 2020)

Lund, J.W., Boyd, T.L. (2016) 'Direct utilization of geothermal energy 2015 worldwide review', *Geothermics* 60, pp. 66-93

Luo, J., Rohn, J., Bayer, M., Priess, A., Wilkmann, L., Xiang, W. (2015) 'Heating and cooling performance analysis of a ground source heat pump system in Southern Germany', *Geothermics* 53, 57–66

Mendrinos, D. and Karytsas, C. (2016) 'Monitoring results after 12 months of provision of heating and cooling at the 8 demonstration buildings of the European project "Ground-Med"', *Conference: European Geothermal Congress (EGC 2016).*[Online] Available at: https://www.researchgate.net/publication (Accessed April 2020)

Mermoud, F., Hollmuller, P., Pampaloni, E., Fraga, C.D., and Lachal, B.M. (2014) 'In situ monitoring results of an existing geothermal heat pump for the heating of a retrofitted office

building in Geneva', *11th International Energy Agency Heat Pump Conference*, [Online] Available at: https://www.researchgate.net/publication (Accessed April 2020)

Miara, M. and Kramer, T. (2011) 'Heat Pump Efficiency Analysis and Evaluation of Heat Pump Efficiency in Real-life Conditions Abbreviated Version', *Fraunhofer ISE* [Online] Available at: https://www.semanticscholar.org (Accessed April 2020)

Michopoulos, A., Bozis, D., Kikidis, P., Papakostas, K., Kyriakis, N.A. (2007) 'Three-years operation experience of a ground source heat pump system in Northern Greece'. *Energy and Buildings* 39, 328–334

Michopoulos, A., Zachariadis, T., Kyriakis, N. (2013) 'Operation characteristics and experience of a ground source heat pump system with a vertical ground heat exchanger', *Energies* 51, pp. 349-357

Naicker, S.S., Rees, S.J. (2018) 'Performance analysis of a large geothermal heating and cooling system', *Renewable Energy* 122, 429-442

Naicker, S.S., Rees, S.J. (2019) 'Long-term high frequency monitoring of a large borehole heat exchanger array', *Renewable Energy* 145, 1528-1542

Nordman, R., Zottl, A. (2011) 'SEPEMO-Build - a European project on seasonal performance factor and monitoring for heat pump systems in the building sector', *REHVA Journal* – August 2011 [Online] Available at: http://sepemo.ehpa.org/fileadmin/red/Deliverables/WP6/D_6_9_SEPEMO_Build_-_Articel_to_REHVA_Journal_Print.pdf (Accessed April 2020)

Nordman, R.; Kleefkens, O.; Riviere, P.; Nowak, T.; Zottl, A.; Arzano-Daurelle, C.; Lehmann, A.; Polyzou, O.; Karytsas, K.; Riederer, P.; et al. (2012) 'SEPEMO—Seasonal Performance Factor and monitoring for HeatPump Systems in the Building Sector', *SP Technical Research Institute of Sweden: Borås, Sweden.* [Online] Available at: https://ec.europa.eu/energy/intelligent/projects/en/projects/sepemo-build (Accessed April 2020)

Pérez-Lombard, L., Ortiz, J., Pout, C. (2008) 'A review on buildings energy consumption information', *Energy and Buildings* 40, 394–398

Sanner, B., (2019) 'Summary of EGC 2019 Country Update Reports on Geothermal Energy in Europe', *European Geothermal Congress 2019 Den Haag*, The Netherlands, 11-14 June 2019. [Online] Available at: http://sepemo.ehpa.org/fileadmin/red/Deliverables/WP6/D_6_9_SEPEMO_Build_-_Articel_to_REHVA_Journal_Print.pdfhttp://europeangeothermalcongress.eu/wp-content/uploads/2019/07/CUR-00-Summary-Europe.pdf (Accessed April 2020)

Shin, J.-H., Cho, Y.-H. (2018) 'Development of a variable water flow rate control method for the circulation pump in a geothermal heat pump system', *Energies* 11 (4),718

SMHI, (2020) *Sveriges meteorologiska och hydrologiska institutem, history weather data log, viewed at 11* [Online] Available at: http://www.smhi.se/data/meteorologi/temperatur (Accessed April 2020)

Spitler, J.D., Javed, S. and Ramstad, R.K. (2016) 'Natural convection in groundwater-filled boreholes used as ground heat exchangers', *Applied Energy*, 164, pp.352-365

Spitler, J.D., Gehlin, S. (2019) 'Measured Performance of a Mixed-Use Commercial-Building Ground Source Heat Pump System in Sweden', *Energies* 12(10),2020

Stafford, A. (2011) 'Long-term monitoring and performance of ground source heat pumps', *Building Research and Information*, 39:6, 566-573

Tsagarakis, KP, Efthymiou, L, Michopoulos, A, Mavragani, A, Anđelković, AS, Antolini, F, Bacic, M, Bajare, D, Baralis, M, Bogusz, W, Burlon, S, Figueira, J, Genç, MS, Javed, S, Jurelionis, A, Koca, K, Ryżyński, G, Urchueguia, JF and Žlender, B (2020) 'A review of the legal framework in shallow geothermal energy in selected European countries: Need for guidelines', *Renewable Energy*, vol. 147, no. Part 2, pp. 2556-2571

Urchueguía, J.F., M. Zacarés, J.M. Corberán, Á. Montero, J. Martos., H. Witte. (2008) 'Comparison between the Energy Performance of a Ground Coupled Water to Water Heat Pump System and an Air to Water Heat Pump System for Heating and Cooling in Typical Conditions of the European Mediterranean Coast', *Energy Conversion and Management* 49, 2917–23

Verein Deutscher Ingenieure (VDI) (2001) *VDI 4640 Thermal Use of the Underground*. Part 932 2: Ground source heat pump systems. Berlin: VDI.

Vieira, A., Alberdi-Pagola, M., Christodoulides, P., (...), Poulsen, S.E., Radioti, G. (2017) 'Characterisation of Ground Thermal and Thermo-Mechanical Behaviour for Shallow Geothermal Energy Applications', *Energies* 10 (12), 2044

Wemhoener, C., Schwarz, R., Rominger, L. (2017) 'IEA HPT Annex 49-Design and integration of heat pumps in nZEB', *Energy Procedia* 122, pp. 661-666

Yu, X., Wang, R.Z., Zhai, X.Q. (2011) 'Year-round experimental study on a constant temperature and humidity air-conditioning system driven by ground source heat pump', *Energies* 36, 1309–1318

Zhai, X.Q., Yang, Y. (2011) 'Experience on the application of a ground source heat pump system in an archives building', *Energy and Buildings* 43(11), pp. 3263-3270

LUND UNIVERSITY

Dept of Architecture and Built Environment: Division of Energy and Building Design
Dept of Building and Environmental Technology: Divisions of Building Physics and Building Services